AFRL-SR-BL-TR-98-

G3164

REPORT DOCUMENTATION PAGE

1. AGENCY USE ONLY (Leave blank)	2. REPORT DATE	3. REPORT TYPE AND DATES COVERED
	MARCH 31, 1998	FINAL TECHNICAL: 9/1/96 - 12/31/97

4. TITLE AND SUBTITLE
(U) MECHANISMS OF UNSTEADY FLOW IN SCRAMJET COMBUSTORS

5. FUNDING NUMBERS
PE - 61102F
PR - 2308
SA - BS
G - F49620-96-1-0435

6. AUTHOR(S)
FRANK E. MARBLE
CHRISTOPHER P. CADOU

7. PERFORMING ORGANIZATION NAME(S) AND ADDRESS(ES)
CALIFORNIA INSTITUTE OF TECHNOLOGY
PASADENA, CA 91125

8. PERFORMING ORGANIZATION REPORT NUMBER

9. SPONSORING/MONITORING AGENCY NAME(S) AND ADDRESS(ES)
AFOSR/NA
110 Duncan Avenue, Suite B115
Bolling AFB DC 20332-0001

10. SPONSORING/MONITORING AGENCY REPORT NUMBER

11. SUPPLEMENTARY NOTES

19980430 085

12a. DISTRIBUTION/AVAILABILITY STATEMENT
Approved for public release; distribution is unlimited

12b. DISTRIBUTION CODE

13. ABSTRACT *(Maximum 200 words)*

This report covers analytic and experimental gasdynamic studies relevant to stability issues of the scramjet supersonic combustion chamber. Its intended purpose was to search for small amplitude very short time scale precurser signals which eventually grew into combustor flow instability, but at a much longer time scale than the signal itself, and consequently offer possibility of control before amplitudes got out of hand. The experiments were done in a basic 2.5 Mach number stream with an artificially thickened boundary layer corresponding to the ingested ramp boundary layer that occurs in the usual installation . A disturbance produced downstream by a small shock tube discharging normally to the gas flow successfully disgorged the shock structure; time resolved pressure and Schlieren image records were obtained. Because upstream signal propagation through the subsonic boundary layer of a supersonic flow is seen as an important issue in the phenomenon under investigation, a rudamentary analytic model was developed. It consists of an acoustically compact element, in which mixing and heat release may occur, with long constant area ducts upstream and downstream of this element. It employs a two stream one dimensional approximation, the main supersonic stream and a subsonic second stream representing the thick boundary layer. Conditions under which interfacial disturbances may be propagated upstream are examined through several examples.

14. SUBJECT TERMS	15. NUMBER OF PAGES
SCRAMJET; SUPERSONIC COMBUSTOR	54
	16. PRICE CODE

17. SECURITY CLASSIFICATION OF REPORT	18. SECURITY CLASSIFICATION OF THIS PAGE	19. SECURITY CLASSIFICATION OF ABSTRACT	20. LIMITATION OF ABSTRACT
Unclassified	Unclassified	Unclassified	UL

MECHANISMS OF UNSTEADY FLOW IN SCRAMJET COMBUSTORS

AFOSR Grant F49620-96-1-0435

Frank E. Marble and Christopher P. Cadou

Final Report

March 31, 1998

California Institute of Technology

Pasadena, California 91125

1. ABSTRACT

This report covers analytic and experimental gasdynamic studies relevant to stability issues of the scramjet supersonic combustion chamber. Its intended purpose was to search for small amplitude very short time scale precurser signals which eventually grew into combustor flow instability, but at a much longer time scale than the signal itself, and consequently offer possibility of control before amplitudes got out of hand. The experiments were done in a basic 2.5 Mach number stream with an artificially thickened boundary layer corresponding to the ingested ramp boundary layer that occurs in the usual installation . A disturbance produced downstream by a small shock tube discharging normally to the gas flow successfully disgorged the shock structure; time resolved pressure and Schlieren image records were obtained. Because upstream signal propagation through the subsonic boundary layer of a supersonic flow is seen as an important issue in the phenomenon under investigation, a rudamentary analytic model was developed. It consists of an acoustically compact element, in which mixing and heat release may occur, with long constant area ducts upstream and downstream of this element. It employs a two stream one dimensional approximation, the main supersonic stream and a subsonic second stream representing the thick boundary layer. Conditions under which interfacial disturbances may be propagated upstream are examined through several examples.

2. INTRODUCTION

There exist boundaries in the paramater space of scramjet operation which, when crossed, result in gross changes of the flowfield. These boundaries in the operating envelope may be associated with i)a major reconfiguration of the combustor inlet shock structure, ii)a restructuring of the flame spreading and stabilization process that leads to flame-out, and iii)the onset and growth of combustion instability. It is suggested that these major flow reconfigurations grow from very small disturbances, of gasdynamic and combustion origin, having a time scale below one millisecond, and diverge over a much longer time scale to produce the observed large flow modifications. Combustion instability, laminar instability and compressor stall, which have some similar properties, exhibit familiar precursor phenomena which, among other things, offer the possibility of control during divergence on the long time scale.

The present work, as originally proposed, was an effort to identify and characterize such precursor signals in the scramjet instability problem. As such it was to include gasdynamic studies in the GALCIT Mach 2.5 wind tunnel, subsequent combustion investigations in the Unsteady Combustion Facility, and analytical studies of signal propagation through subsonic boundary layers of an otherwise supersonic stream. Two significant events severely altered these plans. The first was the decision within GALCIT to proceed with a much needed renovation of the old Guggenheim Aeronautical Laboratory. The schedule for this work took the Mach 2.5 tunnel out of service well ahead of the planned occupancy. The second was the unfortunate death of one of the essential participants, Professor Edward E. Zukoski. His absence retarded progress of the gasdynamic research and rendered the experimental combustion research inadvisable.

As a consequence of this situation it was proposed by the Principal Investigator, and decided with the concurrence of the Program Manager, to reduce both the scope and the financial support of the work and to accomplish as much as possible under an abbreviated schedule. This report covers this work in reasonable detail. Because of the conditions under which is was carried out, it lacks the coherence that was initially intended and consists of two distinct parts, some gasdynamic studies and the rudiments of the analysis that was to guide and interpret both extensive wind tunnel work and the combustion studies. But, as will appear, each portion has developed techniques and produced results that could benefit future work. The analysis and the experiments are covered individually and, because neither is fully developed, no attempt has been made pursue their interaction.

3. ANALYTICAL STUDIES

The following analysis considers a simple model of the scramjet inlet and combustor and asks whether it contains the features necessary for demonstrating a precursor to an inlet instability. Because the thick low speed layer ingested from the ramp is considered to be an essential factor in the unsteady behavior of the device, a two-stream model of the flow represents the greatest degree of simplification that can be tolerated. The model consists of three elements:1. a constant area duct, 2. a compact diffuser/burner, and 3. a constant area duct downstream of the compact element. The upstream and downstream ducts are parallel walled two dimensional channels. In each, the undisturbed flow contains two inviscid streams. In general, one stream represents the main flow in the combustor and is supersonic, the other corresponds to the ingested boundary layer and is subsonic. The common interface between these streams supports no pressure difference and as a consequence the pressure is constant across the entire duct.

The intervening section represents the inlet diffuser and the heat release portion of the flow. Because of the pressure rise accompanying the diffusion process, the subsonic "boundary layer" is physically dragged through this pressure gradient by the interfacial shear. In the model this is represented by a mass, momentum and energy exchange at the interface of magnitude that can be controlled to represent a physically realizable situation.

Small amplitude waves generated in either the upstream or downstream duct may or may not propagate through the central element into the other duct depending upon the mixed flow fields in each duct, the magnitude of the pressure rise, and the mixing processes in the central element. The following sections indicate how these questions were addressed.

Plane Waves in Constant Area Ducts

The flow in each stream of each duct is isentropic and therefore the unsteady disturbances are determined by the equation of motion in the x-direction and the equation of continuity. Because of the unsteady interface between the two streams the forms of these equations are most directly obtained by integrating each equation across each stream. The generic equations of continuity and motion may then be written

$$\frac{\partial \rho}{\partial t} + \frac{\partial}{\partial x}(\rho u) + \frac{\rho}{A}\left(\frac{\partial}{\partial t} + u\frac{\partial}{\partial x}\right)A = 0 \qquad 1.$$

$$\frac{\partial u}{\partial t} + u\frac{\partial u}{\partial x} + \frac{1}{\rho}\frac{\partial p}{\partial x} = 0 \qquad 2.$$

where ρ, u, A have values pertaining to the element and the stream to which they refer. For example, in the high velocity stream of element 3 the variables are $\rho(1,3)$, $u(1,3)$ and $A(1,3)$. The pressure is uniform across the entire duct so that $p(1,3) = p(2,3) \equiv p(3)$.

To obtain the perturbation equations for acoustic analysis, write the variables in the form $\rho + \rho'$, $u + u'$, $p + p'$, where the primed quantities are assumed small. Equations 1 and 2 are

satisfied identically for the steady state values and the first order perturbation equations become

$$\left(\frac{\partial}{\partial t} + u\frac{\partial}{\partial x}\right)\left(\frac{p'}{\gamma p}\right) + u\frac{\partial}{\partial x}\left(\frac{u'}{u}\right) + \left(\frac{\partial}{\partial t} + u\frac{\partial}{\partial x}\right)\frac{A'}{A} = 0 \qquad 3.$$

$$\left(\frac{\partial}{\partial t} + u\frac{\partial}{\partial x}\right)\left(\frac{u'}{u}\right) + \frac{1}{M^2}\, u\frac{\partial}{\partial x}\left(\frac{p'}{\gamma p}\right) = 0 \qquad 4.$$

where M denotes the Mach number of the undisturbed stream in question.

Now consider the upstream duct, element 1. The time dependent disturbances in element 1 are described by two equations of the form 3 and two corresponding equations of the form 4. The specific independent variables are $p'(1)/p(1)$, $u'(1,1)/u(1,1)$, $u'(2,1)/u(2,1)$, $A'(1,1)/A(1,1)$, and $A'(2,1)/A(2,1)$. But because the total duct dimension is fixed, the area perturbations $A'(1,1)$ and $A'(2,1)$ are equal and opposite, we need consider only one of them, namely $A'(2,1)$ the area disturbance of the boundary layer region. As a consequence there is a set of four homogeneous, linear differential equations and four unknown functions.

Anticipating the wave solutions which are of interest, write the proposed solutions in the form

$$\frac{p'(1)}{\gamma p(1)} = P(1)e^{i(\varpi t + kx)} \qquad 5.$$

$$\frac{u'(1,1)}{u(1,1)} = U(1,1)e^{i(\varpi t + kx)} \qquad 6.$$

$$\frac{u'(2,1)}{u(2,1)} = U(2,1)e^{i(\varpi t + kx)} \qquad 7.$$

$$\frac{A'(2,1)}{A(2,1)} = D(2,1)e^{i(\varpi t + kx)} \qquad 8.$$

Substitution into the four differential equations described above yields a set of four homogeneous algebraic equations, whose coefficients must have a vanishing determinant to assure a non-trivial solution.

Define the quantity

$$K = \frac{k\,u(1,1)}{\varpi} \qquad 9.$$

and the algebraic equations may be written

$$(1+K)P(1) + KU(1,1) - (1+K)\frac{A(2,1)}{A(1,1)} D(1,1) = 0 \qquad 10.$$

$$\frac{K}{M^2(1,1)} P(1) + (1+K)U(1,1) = 0 \qquad 11.$$

$$(1+\frac{u(2,1)}{u(1,1)} K)P(1) + \frac{u(2,1)}{u(1,1)} KU(2,1) + (1+\frac{u(2,1)}{u(1,1)} K) D(2,1) = 0 \qquad 12.$$

$$\frac{K}{M^2(2,1)} \frac{u(2,1)}{u(1,1)} P(1) + (1+\frac{u(2,1)}{u(1,1)} K)U(2,1) = 0 \qquad 13.$$

the vanishing determinant of which yields a quartic in K.

There are then four complex roots of K for each set of parameters in element 1 and four values for each set of parameters in element 3. Therefore we define

$$K(i,j) = R(i,j) + iS(i,j) \qquad 14.$$

for i = 1 to 4 and j = 1 or 3, where R(i,j) and S(i,j) are real. The solutions for the time dependent perturbation flows in each element are then the sum of four terms, one corresponding to each of the appropriate roots. For example, the pressure perturbation in element 1 may be written explicitly as

$$\frac{p'(1)}{\gamma p(1)} = \sum_{i=1}^{4} P(i,1)\, e^{i\varpi(t+K(i,1)\frac{x}{u(1,1)})} \qquad 15.$$

where now the P(i,j) are the coefficients for the individual pressure waves in each element j = 1 and j = 3. These coefficients are determined, as in conventional acoustics problems, from the upstream and downstream conditions imposed upon the solution. The solutions for the velocity and area perturbations of each stream in the element may be written down in a similar manner. In each case the coefficients of the expansion may be determined from the P(i,j)'s from any three of equations 10 through 13.

Flow in the Central Element

Within the central element the flow processes include not only the area change of the complete duct but also the mixing interaction of the two streams. To avoid unreasonable complication and still retain reasonable accuracy, the flow through the central element is divided into two steps. The first is a flow at constant area within which mass, momentum and energy are exchanged between the two streams. In the second step the area change associated with the pressure rise is carried out treating each stream as isentropic. The accuracy of this

approximation becomes questionable only when the pressure ratio is quite large and in this circumstance the pair of steps may be repeated, using a small pressure rise in each step. The constant area mixing step will be treated as going between element 1 and element 2. The isentropic step will be designated as going from element 2 to element 3.

The flow in stream 1 during the mixing process is described by the familiar one dimensional equations of continuity, momentum and energy. There is, as will be recognized, a degree of arbitrariness in defining the individual high velocity and low velocity streams during the mixing process. As a matter of convenience the mass flow in each stream tube will be taken as constant, that is, the mass of gas transferred from stream 1 to stream 2 is, at any point, identical with that transferred from stream 2 to stream 1. Thus the equation of continuity for stream 1 is simply

$$\rho(1,1)\, u(1,1) A(1,1) = \rho(1,2)\, u(1,2) A(1,2) = m(1)$$

where $A(1,1) = A(1,2)$ because of the constant area assumption of this step. In writing the equation of momentum conservation it is assumed that a mass $\mu\, m(1)$ is transferred from stream 1 to stream 2 carrying with it the momentum and the energy of stream 1. Correspondingly, the same mass is transferred from stream 2 to stream 1 again carrying with it the momentum and energy characterizing stream 2. Then defining

$$\alpha(1) = \mu \left(\frac{u(1,1)-u(1,2)}{u(1,1)}\right) \qquad 16.$$

the momentum equation may be written as

$$\frac{p(1,2)}{p(1,1)} = 1 + \gamma M^2(1,1)\left(1 - \frac{u(1,2)}{u(1,1)} - \alpha(1)\right) \qquad 17.$$

If, further, the quantity $\beta(1)$ is defined

$$\beta(1) = \mu\left(\frac{T_s(1,1) - T_s(1,2)}{T_s(1,1)}\right) \qquad 18.$$

the energy equation becomes

$$\left(\frac{p(1,2)}{p(1,1)} + \frac{\gamma-1}{2} M^2(1,1)\left(\frac{u(1,2)}{u(1,1)}\right)\right)\frac{u(1,2)}{u(1,1)} = (1-\beta(1))\left(1+\frac{\gamma-1}{2} M^2(1,1)\right) \qquad 19.$$

Note that equations 17 and 19 may be solved for the pressure ratio and the velocity ratio; the equation 4.16 then gives the density ratio so that the solution is completely known at position 2.

The solution for stream 2, the low velocity stream, proceeds in a similar manner. The equation of continuity is

$$\rho(2,1)\, u(2,1) A(2,1) = \rho(2,2)\, u(2,2)\, A(2,2) = m(2) \qquad 20.$$

where again $A(2,1) = A(2,2)$. The momentum equation becomes

$$\frac{p(2,2)}{p(2,1)} = 1 + \gamma M^2(2,1)\left(1 - \frac{u(2,2)}{u(2,1)} + \alpha(2)\right) \qquad 21.$$

where the momentum exchange term $\alpha(2)$ is

$$\alpha(2) = \alpha(1)\left(\frac{m(1)}{m(2)}\right)\left(\frac{u(1,1)}{u(2,1)}\right) \qquad 22.$$

and because of the velocity and mass flow ratios, this is usually much larger than $\alpha(1)$. The energy equation for stream 2 is modified correspondingly

$$\left(\frac{p(2,2)}{p(2,1)} + \frac{\gamma - 1}{2} M^2(2,1)\left(\frac{u(2,2)}{u(2,1)}\right)\right)\left(\frac{u(2,2)}{u(2,1)}\right) = \left(1 + \beta(2)\right)\left(1 + M^2(2,1)\right) \qquad 23.$$

where $\beta(2)$, the energy exchange term, is

$$\beta(2) = \beta(1)\left(\frac{m(1)}{m(2)}\right)\left(\frac{T_s(1,1)}{T_s(2,1)}\right) \qquad 24.$$

This set of equations for stream 2 likewise permits solution for the complete gas state at element 2.

This state is not, however, the condition at which the gas enters the downstream duct, element 3, because the pressures of stream 1 and stream 2 are not equal. The issue is now to select the desired pressure downstream of the mixer and expand both streams to this common value. The most direct manner to carry this out is to recognize that the pressure p(1,3) (=p(3)) is known and calculate the Mach number M(1,3) in the downstream duct. this gives directly

$$M^2(1,3) = \frac{2}{\gamma - 1}\left(\left(\frac{p(1,2)}{p(1,3)}\right)^{\frac{\gamma-1}{\gamma}}\left(1 + \frac{\gamma - 1}{2} M^2(1,2)\right) - 1\right) \qquad 25.$$

from which the remaining conditions for stream 1 in element 3 follow

$$\frac{T(1,3)}{T(1,2)} = \frac{1 + \frac{\gamma - 1}{2} M^2(1,2)}{1 + \frac{\gamma - 1}{2} M^2(1,3)} \qquad 26.$$

$$\frac{u(1,3)}{u(1,1)} = \left(\frac{M(1,3)}{M(1,1)}\right)\sqrt{\frac{T(1,3)}{T(1,1)}} \qquad 27.$$

A set of equations completely similar to 25 through 27 give the conditions of stream 2 in

element 3 and are obtained by simply changing the first index in each variable from 1 to 2, recalling that p(1,3) = p(2,3) and is a prescribed value.

Because the pressure rise across the central element is prescribed, the areas of the two streams in element 3 must be calculated from the known mass flow rates and discharge gas state from the central element. Using the equation of continuity, the flow area of the high velocity stream in element 3 is

$$A(1,3) = A(1,1)\left(\frac{p(1,1)}{p(1,3)}\right)\left(\frac{T(1,3)}{T(1,1)}\right)\left(\frac{u(1,1)}{u(1,3)}\right) \qquad 28.$$

Similarly, the velocity of the low velocity stream in element 3 is

$$A(2,3) = A(2,1)\left(\frac{p(2,1)}{p(2,3)}\right)\left(\frac{T(2,3)}{T(2,1)}\right)\left(\frac{u(2,1)}{u(2,3)}\right) \qquad 29.$$

Unsteady Flow in Central Element and Matching with Elements 1 and 3

The complete system consists of the three elements and to determine the unsteady behavior of the system requires analysis of the unsteady response of the central element and the subsequent matching with the waves in elements 1 and 3, the solutions for which have been obtained earlier. To accomplish this the central element will be considered acoustically compact, that is, the phase difference between related disturbances at the inlet and outlet will be neglected. There are certainly circumstances for which this approximation is inaccurate and they will be pointed out but not analyzed further. The consequence of the compactness assumption is that the steady flow relationships that have been developed between states 1 and 2, and between states 2 and 3, may be perturbed without carrying out a complete wave analysis of the central element.

It is convenient to describe the interface between states 1 and 2, for the high and low velocity streams, through perturbation of the momentum and energy relations. Working from equation 17, which relates states 1 and 2 in stream 1, the appropriate first order momentum perturbation is

$$a_{11}\left(\frac{p'(1,1)}{p(1,1)}\right) + a_{12}\left(\frac{u'(1,1)}{u(1,1)}\right) + a_{13}\left(\frac{u'(2,1)}{u(2,1)}\right) = b_{11}\left(\frac{p'(1,2)}{p(1,2)}\right) + b_{12}\left(\frac{u'(1,2)}{u(1,2)}\right) \qquad 30.$$

where the coefficients are given in terms of the known steady state variables

$$a_{11} = 1 + M^2(1,1)\left[1 - \frac{u(1,2)}{u(1,1)} - \alpha(1)\right] \qquad 31.$$

$$a_{12} = M^2(1,1)\left[1 - \frac{u(1,2)}{u(1,1)} - \alpha(1) + 1 - \mu\right] \qquad 32.$$

$$a_{13} = M^2(1,1)\,\mu\,\frac{u(2,,1)}{u(1,1)} \qquad 33.$$

$$b_{11} = \frac{p(1,2)}{p(1,1)} \qquad 34.$$

$$b_{12} = M^2(1,1)\,\frac{u(1,2)}{u(1,1)} \qquad 35.$$

There are three more perturbation equations at this interface, one for energy matching in stream 1 and one each for momentum and energy matching In stream 2. Likewise there are four perturbation equations at the interface 2 - 3.

The matching equations at the interface 1 - 2 and those at the interface 2 - 3 each contain the four perturbation variables $u'(1,2)$, $u'(2,2)$, $p'(1,2)$, and $p'(2,2)$. Therefore, among these eight equations the perturbation variables referring to element 2 may be eliminated algebraically. The four resulting equations thus link elements 1 and 3 directly. These relations contain the perturbation variables $u'(1,1)$, $u'(2,1)$, $p'(1,1) \equiv p'(2,1)$, $A'(1,1) \equiv -A'(2,1)$ referring to element 1, and the perturbation variables $u'(1,3)$, $u'(2,3)$, $p'(1,3) \equiv p'(2,3)$, $A'(1,3) \equiv -A'(2,3)$.

Solution for the Pressure Waves

It will be recalled that the upstream duct, element 1, and the downstream duct, element 3, each supported four waves distinguished by the complex wave numbers, equation 4.9. These characteristic wave numbers establish the speed and growth rate of each of the four waves in each element. And, as illustrated by equation 15, the solution for any of the perturbation variables in either element consists of a linear sum of the appropriate waves. If one of these elements existed in isolation the magnitude of each wave would be determined by conditions at the duct ends, similar to the situation for conventional acoustics of a constant area duct. Exactly what may be prescribed at either end depends upon whether the wave is propagating to the right or to the left.

In the present example, element 1 terminates at the compact element 2 and consequently one is not free to prescribe conditions there. The amplitude and phase of any wave that propagates to the left, or upstream, in element 1 must be determined at the interface 1 - 3, that is by the matching relations developed in the preceeding section. On the other hand, waves in element 1 that propagate downstrean may be prescribed conventionally at the left end of that duct. Conversely, the downstream propagating waves in element 3 are determined by the matching conditions at the interface 1 - 3 but upstream propagating waves may be prescribed. The wave velocities in each element are established by the undisturbed flow conditions in each element. The conditions to be prescribed, on the other hand, are fixed by the physical problem under consideration. To fix these ideas, consider a situation appropriate to a scramjet combustor. Suppose that in both elements 1 and 3, three waves propagate downstream and one wave propagates upstream. In the upstream region one is free to prescribe that no disturbances enter the diffuser, that is to set the amplitudes of the three appropriate waves to zero, leaving one undetermined wave in the inlet duct. Since it is an upstream propagating wave in the supersonic main flow it is reasonable to suppose this wave is mainly propagating in the boundary layer, that is, in the low velocity stream 2. In the duct downstream of the diffuser, however, three of the waves, those propagating downstream, are determined by the matching conditions at the interface and the one remaining wave propagating upstream may be prescribed. Prescribing a value for this wave is the physical equivalent of creating a disturbance in the combustion chamber and the corresponding result of physical interest is whether, and in what magnitude, the diffuser/mixer element, described by the matching conditions at the 1 - 3 interface, allow this disturbance to propagate into the approach flow. From a mathematical standpoint, there is a total of eight waves, four have been prescribed by physical conditions remote from the diffuser, the amplitudes and phases of the remaining four are determined by the matching conditions.

The details of carrying through these calculations are both involved and tedious but are largely a matter of careful bookkeeping. The solutions for the velocity, pressure and area perturbations, equations 5 to 8 and a corresponding set for element 3, are required for satisfying the matching conditions, e.g equation 30. But recall that while the roots of the determinant of the algebraic set 10 through 13 give the complex wave numbers for the solutions, there remain three of these equations that provide relationships between P(1), U(1,1), U(2,1), and D(1,1). Therefore the quantities U(1,1), U(2,1) and D(1,1) may be expressed in terms of the pressure perturbations, P(1). For example from equation 11

$$U(1,1) = -\frac{1}{M^2(1,1)} \frac{K}{1+K} P(1) \qquad 36.$$

and the others follow from the remaining equations. Because the K values, equation 14, are complex, the coefficients in solutions 5 through 8 are complex. But because it is now seen necessary only to deal with the pressure waves, they may be written P(i,j) + i Q(i,j) where the indices i, j have the same meaning as for the wave numbers K(i,j), equation 14. The solution for the pressure perturbation in element 1, replacing that written in equation 15, is

$$\frac{p'(1)}{\gamma p(1)} = \sum_{i=1}^{4} (P(i,1) + iQ(i,1)) e^{i\varpi\left[t+(R(i,1)+iS(i,1))\frac{x}{u(1,1)}\right]} \qquad 37.$$

and a corresponding solution can be written for element 3 by simply replacing the index 1 by 3 where appropriate. It is now clear that the four complex matching conditions yield eight real relations and that the unknown real coefficients P(i,j) , Q(i,j) number 16. Each prescription of a physical radiation condition, far upstream or downstream, provides two coefficients, the amplitude and phase. And since the matching conditions now provide eight additional coefficients, one is at liberty to specify four complex, (eight real) radiation conditions. Once the "accounting" for the elements 1 and 3 is complete, only the inversion of an 8×8 matrix is involved.

Some Results of Calculations

The analysis described in the foregoing sections allows calculations of the unsteady flow to be made in two steps. First, the four complex wave numbers and wave speeds must be calculated for each of the two duct elements. This is a necessary first step because, as explained above, this information determines which radiation conditions must be prescribed at points far upstream and downstream from the diffuser. Second, after prescribing the physically appropriate radiation conditions for element 1 and for element 3, the matching matrix is inverted to obtain the wave amplitudes and phases in both elements. The issue of prime physical significance here is the propagation of an upstream moving wave in element 3, through the diffuser mixer element into element 1. If this occurs, it corresponds to the propagation of a disturbance through the boundary layer of a supersonic stream into the flow entering the diffuser. As should be expected, the upstream propagation of a small disturbance will occur for only certain combinations of boundary layer thickness, boundary layer Mach number and values of other steady state flow variables.

Examples of the wave number and wave speed calculations are given below.

Example 1.

Calculations of Wave Numbers and Wave Speeds

Flight Conditions

Flight Mach Number	7.5
Outside Air Temperature	400 R
Free Stream Stagnation Temperature	4900 R

Inlet Conditions, Element 1

Mach Number, High Velocity Stream	2.5
Mach Number, Low Velocity Stream	0.3
Boundary Layer Area Ratio, A(2,1)/A(1,1)	0.01
Stagnation Temperature, Stream 3	4900 R
Mass Flow Ratio, m(2)/m(1)	8.07E-04

Complex Wave Numbers

R(1,1)	-0.715
S(1,1)	0.000
R(2,1)	-1.672
S(2,1)	0.000
R(3,1)	-4.030
S(3,1)	0.000
R(4,1)	-8.912
S(4,1)	0.000

Wave Speeds

$\frac{V}{u(1,1)}(1)$	1.398
$\frac{V}{u(1,1)}(2)$	0.598
$\frac{V}{u(1,1)}(3)$	0.248
$\frac{V}{u(1,1)}(4)$	0.122

Example 2.

Calculations of Wave Numbers and Wave Speeds

Flight Conditions

Flight Mach Number	7.5
Outside Air Temperature	400 R
Free Stream Stagnation Temperature	4900 R

Inlet Conditions, Element 1

Mach Number, High Velocity Stream	2.5
Mach Number, Low Velocity Stream	0.3
Boundary Layer Area Ratio, A(2,1)/A(1,1)	0.1
Stagnation Temperature, Stream 3	4900 R
Mass Flow Ratio, m(2)/m(1)	8.07E-03

Complex Wave Numbers

R(1,1)	-0.722
S(1,1)	0.000
R(2,1)	-1.750
S(2,1)	0.000
R(3,1)	66.339
S(3,1)	0.000
R(4,1)	-2.411
S(4,1)	0.000

Wave Speeds

$\frac{V}{u(1,1)}(1)$	1.386
$\frac{V}{u(1,1)}(2)$	0.571
$\frac{V}{u(1,1)}(3)$	-0.015
$\frac{V}{u(1,1)}(4)$	0.415

Example 3.

Calculations of Wave Numbers and Wave Speeds

Flight Conditions

Flight Mach Number	7.5
Outside Air Temperature	400 R
Free Stream Stagnation Temperature	4900 R

Inlet Conditions, Element 1

Mach Number, High Velocity Stream	2.5
Mach Number, Low Velocity Stream	0.3
Boundary Layer Area Ratio, A(2,1)/A(1,1)	0.2
Stagnation Temperature, Stream 3	4900 R
Mass Flow Ratio, m(2)/m(1)	1.61E-02

Complex Wave Numbers

R(1,1)	-0.728
S(1,1)	0.000
R(2,1)	12.566
S(2,1)	0.000
R(3,1)	-1.853
S(3,1)	0.228
R(4,1)	-1.853
S(4,1)	-0.228

Wave Speeds

$\frac{V}{u(1,1)}(1)$	1.373
$\frac{V}{u(1,1)}(2)$	-0.080
$\frac{V}{u(1,1)}(3)$	0.540
$\frac{V}{u(1,1)}(4)$	0.540

Example 4.

Calculations of Wave Numbers and Wave Speeds

Flight Conditions

Flight Mach Number	7.5
Outside Air Temperature	400 R
Free Stream Stagnation Temperature	4900 R

Inlet Conditions, Element 1

Mach Number, High Velocity Stream	2.5
Mach Number, Low Velocity Stream	0.3
Boundary Layer Area Ratio, A(2,1)/A(1,1)	0.4
Stagnation Temperature, Stream 3	4900 R
Mass Flow Ratio, m(2)/m(1)	3.23E-02

Complex Wave Numbers

R(1,1)	-0.740
S(1,1)	0.000
R(2,1)	6.491
S(2,1)	0.000
R(3,1)	-1.657
S(3,1)	0.336
R(4,1)	-1.657
S(4,1)	-0.336

Wave Speeds

$\frac{V}{u(1,1)}(1)$	1.351
$\frac{V}{u(1,1)}(2)$	-0.154
$\frac{V}{u(1,1)}(3)$	0.604
$\frac{V}{u(1,1)}(4)$	0.604

These examples illustrate the important features of the calculations and the results for wave propagation in a mixed supersonic/ subsonic flow in a duct. First consider Example 2. The example assumes a flight Mach number of 7.5 at an altitude in the range of 60,000 feet; the resulting stagnation temperature is 4900 R. The Mach number of the free stream air entering the engine after retardation by the ramp is 2.5. The boundary layer ingested from the ramp is assumed to occupy 0.1 of the inlet area and is characterized by a Mach number of 0.3 and is assumed to have retained the free stream stagnation temperature. The boundry layer mass flow is consequently 0.008 that of the free stream flow into the engine. The real and imaginary parts of the wave numbers result in two undamped waves and a pair of complex conjugate wave numbers, one of which will result in a divergent solution. The wave speeds show that for the system parameters of this example, three waves propagate downstream and one propagates upstream at about one quarter of the velocity of the main flow through the engine. This wave is the one of interest and is a direct result of the subsonic boundary layer.

The four example calculations illustrate the sensitivity of this forward propagating wave to the magnitude of the boundary layer flow ingested into the engine. The conditions are identical for the examples except for the fraction of the duct flow area occupied by the ingested boundary layer. In the first example the boundary layer flow area ratio, A(2,1)/A(1,1), is equal to 0.01 with the consequence that no pressure wave propagates upstream. As the boundary layer area ratio is increased through the values 0.1 in example 2, 0.2 in example 3 and 0.4 in example 4, the upstream propagating wave appears and increases in velocity as A(2,1)/A(1,1) increases. The examples also illustrate the cut-off phenemon where the smaller amounts of boundary layer air ingested prohibit upstream propagation of pressure waves. Such basic wave calculations are essential to calculating the response of the diffuser/burner model to an input disturbance downstream of the element.

The calculation of unsteady flow in the complete system involves the following components: i)steady flow in the system for prescribed flight and system entrance conditions, mixing rate in the diffuser/burner, and pressure rise from element 1 to element 3, ii)wave solutions for element 1 and element 3, iii)prescription of a pressure disturbance in element 3, iv)propagation of this disturbance upstream through the diffuser/burner into element 1, utilizing the matching conditions for the two sets of pressure waves. An example of the results of a complete system calculation follows.

Example 1.

Calculation of Unsteady Flow in Complete System

Flight Conditions

Flight Mach Number	7.5
Outside Air Temperature	400 R
Free Stream Stagnation Temperature	4900 R

Inlet Conditions, Element 1

Mach Number,High Velocity Stream	2.5
Mach Number, Low Velocity Stream	0.3
Boundary Layer Area Ratio, A(2,1)/A(1,1)	0.5
Stagnation Temperature, Stream 3	2940 R
Mass Flow Ratio, m(2)/m(1)	5.21E-02

Discharge Flow, Compact Element

Mass Exchange Fraction, Stream 1, μ	0.01
Momentum Exchange Fraction, $\alpha(1)$	8.62E-03
Energy Exchange Fraction, $\beta(1)$	0.40E-02
Mass Exchange Fraction, Stream 2, $-\mu m(1)/m(2)$	- 0.19
Momentum Exchange Fraction, $\alpha(2)$	-1.20
Energy Exchange Fraction, $\beta(2)$	-0.13

Conditions in Element 3

Mach Number, High Velocity Stream	2.35
Mach Number, Low Velocity Stream	0.14
Boundary Layer Area Ratio, A(2,3)/A(1,3)	1.05
System Pressure Ratio, p(1,3)/p(1,1)	1.2

Calculation of Complex Wave Numbers

Wave Numbers, Element 1		Wave Numbers, Element 3	
R(1,1)	-.749	R(1,3)	-.763
S(1,1)	0.000	S(1,3)	0.000
R(2,1)	-1.664	R(2,3)	3.297
S(2,1)	0.000	S(2,3)	0.000
R(3,1)	7.173	R(3,3)	-1.761
S(3,1)	0.000	S(3,3)	0.079
R(4,1)	-2.084	R(4,3)	-1.762
S(4,1)	0.000	S(4,3)	-0.079

Example 1, continued.

System Response, Pressure Input in Element 3

Element 1

Wave	V / u(1,1)	p′(1,1) / p(1,1)	u′(1,1) / u(1,1)	u′(2,1) / u(2,1)	A′(2,1) / A(2,1)
1.	1.335	0.000	0.000	0.000	0.000
2.	0.601	0.000	0.000	0000.	0.000
3.	-0.139	0.372	-0.052	-2.059	0.653
4.	0.480	0.000	0.000	0.000	0.000

Element 3

Wave	V / u(1,3)	p′(1,3) / p(1,3)	u′(1,3) / u(1,3)	u′(2,3) / u(2,3)	A′(2,3) / A(2,3)
1.	1.329	-0.716	-0.435	-2.296	-0.939
2.	-0.329	1.000	-0.150	-9.129	0.846
3.	0.549	0.093	0.251	5.024	0.331
4.	0.549	0.116	0.241	5.206	0.342

The pressure disturbance has been entered in stream 1 of element 3 on the only upstream propagating wave, indicated Wave 1 in the tabulation. The Waves 2 - 4 in element 3 all propagate downstream and consequently their amplitudes are determined by the matching conditions at the interface 1-3. Note the velocity and stream area disturbances that accompany the pressure wave input. The stream velocities are retarded by the pressure pulse but the effect on the low velocity stream, $u'(2,3)$, is much stronger, suggesting that a large pulse could separate the boundary layer. The result is to grossly thicken the boundary layer, as indicated by the large value of $A'(2,3)$. Note that the pressure pulse has been given the magnitude unity which allows simple scaling for a physically acceptable value of the pressure perturbation. Because the system is a linear one, all wave amplitudes scale in proportion to the input value of $p'(1,3)$, for example prescribing $p'(1,3)/p(1,3)$ equal to 0.10 would divide all tabulated values by 10.

The tabulated solutions for element 1 show that the pressure disturbance injected into element 3 has passed upstream, through the diffuser/combustor, into the inlet element activating Wave 1, the only one of the set that propagates upstream. The other waves, Waves 2 - 4, have been set to zero amplitude corresponding to the physical choice that no disturbances are put into the system from upstream. Note that, in accordance with the earlier discussion of radiation conditions, four of the total eight waves have been prescribed, three in element 1, one in element 3, leaving four to be determined by the matching conditions. Note that for the linearization that has been employed in the analysis to be valid, all calculated perturbations must be small compared with unity. Inspection of the tabulated values suggests that, for the present example, the value of the pressure disturbance $p'(1,3)/p(1,3)$ should not exceed 0.05. It is significant, and physically evident, that the most sensitive of the perturbation quantities is the velocity perturbation in the low velocity stream. The physical reason is that even a small pressure perturbation in the high velocity stream is a significant fraction of the velocity pressure of the low velocity stream and hence has a large effect on the velocity $u'(2,3)$ of the slower stream. This effect may be noted also in the correspondingly large stream area change $A'(2,3)$.

Two more examples of the system calculation are shown in the following pages to illustrate the effects of changing the mass, momentum, and energy exchange rates, such as could be introduced by enhanced mixing. These enhanced mixing rates also permit a larger pressure rise across the diffuser.

Example 2.

Calculation of Unsteady Flow in Complete System

Flight Conditions

Flight Mach Number	7.5
Outside Air Temperature	400 R
Free Stream Stagnation Temperature	4900 R

Inlet Conditions, Element 1

Mach Number,High Velocity Stream	2.5
Mach Number, Low Velocity Stream	0.3
Boundary Layer Area Ratio, A(2,1)/A(1,1)	0.5
Stagnation Temperature, Stream 3	2940 R
Mass Flow Ratio, m(2)/m(1)	5.21E-02

Discharge Flow, Compact Element

Mass Exchange Fraction, Stream 1, μ	0.02
Momentum Exchange Fraction, $\alpha(1)$	1.72E-02
Energy Exchange Fraction, $\beta(1)$	0.80E-02
Mass Exchange Fraction, Stream 2, $-\mu m(1)/m(2)$	- 0.38
Momentum Exchange Fraction, $\alpha(2)$	-2.39
Energy Exchange Fraction, $\beta(2)$	-0.26

Conditions in Element 3

Mach Number, High Velocity Stream	2.24
Mach Number, Low Velocity Stream	0.14
Boundary Layer Area Ratio, A(2,3)/A(1,3)	1.05
System Pressure Ratio, p(1,3)/p(1,1)	1.35

Calculation of Complex Wave Numbers

Wave Numbers, Element 1		Wave Numbers, Element 3	
R(1,1)	-0.749	R(1,3)	-0.752
S(1,1)	0.000	S(1,3)	0.000
R(2,1)	-1.664	R(2,3)	3.034
S(2,1)	0.000	S(2,3)	0.000
R(3,1)	7.173	R(3,3)	-1.684
S(3,1)	0.000	S(3,3)	0.302
R(4,1)	-2.084	R(4,3)	-1.684
S(4,1)	0.000	S(4,3)	-0.302

Example 2, continued.

System Response, Pressure Input in Element 3

Element 1

Wave	$\frac{V}{u(1,1)}$	$\frac{p'(1,1)}{p(1,1)}$	$\frac{u'(1,1)}{u(1,1)}$	$\frac{u'(2,1)}{u(2,1)}$	$\frac{A'(2,1)}{A(2,1)}$
1.	1.335	0.000	0.000	0.000	0.000
2.	0.601	0.000	0.000	0000.	0.000
3.	-0.139	0.000	0.000	0.000	0.000
4.	0.480	0.000	0.000	0.000	0.000

Element 3

Wave	$\frac{V}{u(1,3)}$	$\frac{p'(1,3)}{p(1,3)}$	$\frac{u'(1,3)}{u(1,3)}$	$\frac{u'(2,3)}{u(2,3)}$	$\frac{A'(2,3)}{A(2,3)}$
1.	1.311	-0.884	-0.516	-2.612	-1.151
2.	-0.303	1.000	-0.139	-9.808	0.849
3.	0.568	-0.074	0.362	4.609	0.279
4.	0.568	0.183	0.256	6.477	0.418

Example 3.

Calculation of Unsteady Flow in Complete System

Flight Conditions

Flight Mach Number	7.5
Outside Air Temperature	400 R
Free Stream Stagnation Temperature	4900 R

Inlet Conditions, Element 1

Mach Number,High Velocity Stream	2.5
Mach Number, Low Velocity Stream	0.3
Boundary Layer Area Ratio, A(2,1)/A(1,1)	0.5
Stagnation Temperature, Stream 3	2940 R
Mass Flow Ratio, m(2)/m(1)	5.21E-02

Discharge Flow, Compact Element

Mass Exchange Fraction, Stream 1, μ	0.03
Momentum Exchange Fraction, $\alpha(1)$	2.59E-02
Energy Exchange Fraction, $\beta(1)$	0.012
Mass Exchange Fraction, Stream 2, $-\mu m(1)/m(2)$	- 0.58
Momentum Exchange Fraction, $\alpha(2)$	-3.59
Energy Exchange Fraction, $\beta(2)$	-0.38

Conditions in Element 3

Mach Number, High Velocity Stream	2.13
Mach Number, Low Velocity Stream	0.13
Boundary Layer Area Ratio, A(2,3)/A(1,3)	1.04
System Pressure Ratio, p(1,3)/p(1,1)	1.5

Calculation of Complex Wave Numbers

Wave Numbers, Element 1		Wave Numbers, Element 3	
R(1,1)	-0.749	R(1,3)	-0.742
S(1,1)	0.000	S(1,3)	0.000
R(2,1)	-1.664	R(2,3)	2.805
S(2,1)	0.000	S(2,3)	0.000
R(3,1)	7.173	R(3,3)	-1.617
S(3,1)	0.000	S(3,3)	0.391
R(4,1)	-2.084	R(4,3)	-1.617
S(4,1)	0.000	S(4,3)	-0.391

Example 3, continued.

System Response, Pressure Input in Element 3

Element 1

Wave	$\frac{V}{u(1,1)}$	$\frac{p'(1,1)}{p(1,1)}$	$\frac{u'(1,1)}{u(1,1)}$	$\frac{u'(2,1)}{u(2,1)}$	$\frac{A'(2,1)}{A(2,1)}$
1.	1.335	0.000	0.000	0.000	0.000
2.	0.601	0.000	0.000	0.000	0.000
3.	-0.139	0.602	-0.087	-3.431	1.088
4.	0.480	0.000	0.000	0.000	0.000

Element 3

Wave	$\frac{V}{u(1,3)}$	$\frac{p'(1,3)}{p(1,3)}$	$\frac{u'(1,3)}{u(1,3)}$	$\frac{u'(2,3)}{u(2,3)}$	$\frac{A'(2,3)}{A(2,3)}$
1.	1.348	-0.404	-0.255	-1.399	-0.533
2.	-0.357	1.000	-0.162	-10.070	0.843
3.	-0.619	0.179	0.109	4.177	0.278
4.	0.619	0.194	0.103	4.300	0.284

4. WIND TUNNEL EXPERIMENTS

It is generally accepted that the process leading to disgorging a shock from a supersonic combustion chamber essentially involves propagation of a disturbance through the boundary layer, a boundary layer that may be unusually thick because of ingesting boundary layer air from the inlet ramp. The gasdynamic experiments were aimed to explore this unsteady process of wave propagation upstream through an artificially thickened boundary layer on one wall of the working section of a supersonic wind tunnel.

Wind Tunnel and Instrumentation

These investigations were carried out in the GALCIT M = 2.5 wind tunnel. This tunnel is a continuous draw down facility taking filtered air at ambient atmospheric conditions and discharging through a two-stage constant displacement vacuum pump. A schematic diagram of the working section, including the extensive modifications to accommodate the present experiment, is shown in Figure 1. The working section, 32 in long, 2.5 in wide, gave ample space for the boundary layer injection and the pulse generator. The splitter plate shown on the upper wall separated the high speed flow in the tunnel from the additional low speed air injected parallel to the main flow to simulate the thick boundary layer. The height of the test section was 1.97 in upstream of the injection plane and 2.375 in downstream. A low loss choked orifice flow meter was used to determine the injected mass flow rate. A throttling valve controled the stagnation pressure upstream of the orifice allowing injection velocities in the range $0.15 < M < 0.9$.

Three high-speed piezoelectric pressure transducers (PCB 112-A21), installed in the duct, numbered 1a, 2a, and 3a in the diagram, detect disturbances propagating through the boundary layer. A fourth, numbered 0a, was installed in the disturbance generator to provide a trigger signal and a time reference for the experiment. The signals from these transducers were amplified (PCB 482-A20) and digitized (Keithley DAS 58) at 250 kHz. At this rate, two pressure transducers spaced one inch apart were sampled 10 times as a disturbance moving with the flow swept over them. It was determined more important to maintain the higher sampling rate than to sample a larger number of transducers less frequently. The digitized pressure data were stored on the host computer's hard drive.

Slower response absolute pressure transducers (Statham PA208TC) labled S1, S2, and S3 measured static pressures upstream and downstream of the choked orifice in addition to various locations on the wall of the test section. Their output was amplified and digitized (Keithley DAS 20) at approximately 10 kHz. The sampling rate was not important here because the static pressure measurements were used only to characterize the steady flow before each unsteady experiment. Fifty samples were averaged for each static pressure measurement and the results written to the host computer's hard disk. A three channel multiplexing valve was used to increase the number of static pressure measurements that could be made during each tunnel run. Table 1 shows the locations and multiplexer assignments for the pitot probe and various static pressure taps. Note that Pin is the tunnel pressure immediately upstream of the vacuum pumps and Patm is the atmospheric pressure

Multiplexer Pos		Unsteady Expts.		
			Static 1	
F	1	Static1	21.75	
	2	Static3	27.75	U
	3	Static4	32.25	U
G	1	Patm		
	2	Up Orf		
	3	Pin		L
H	1	Static2	21.5	L
	2	Dn Orf		
	3	Static5	15.5	L

Table 1. Multiplexer assignments and pressure measurement locations for unsteady experiments.

In addition to the unsteady experiments, pitot tube traverses were made in order to measure the character of the augmented boundary layer and the velocity profile across the test section. Table 2 and Figures 2 and 3 show the locations of the static pressure taps and the pitot probe for profiles measured upstream and downstream of the injection slot. The same absolute pressure transducers (Statham PA208TC) and multiplexing valves used in the unsteady experiments were used here.

A DC motor under computer control drove the pitot probe up and down while a calibrated slide potentiometer provided a voltage by which to measure probe position. Pitot and static pressures were recorded by the computer at each measuring station. Typically 18 measurements were taken across each test section. In addition, the system was capable of triggering the 35-mm camera to record Schlieren images of the steady flow.

Multiplexer Pos		Pitot Traverse 1			Pitot Traverse 2		
			x (in)			x (in)	
F	1	Pin			Static1	21.75	U
	2	Static3	27.75	U	Static3	27.75	U
	3	Static4	21.75	U	Static4	32.25	U
G	1	Static1	32.25	U	Pitot	27.5	L
	2	Up Orf			Up Orf		
	3	Pitot	34.5	L	Pin		
H	1	Static2	27.5	L	Static2	21.5	L
	2	Dn Orf			Dn Orf		
	3	Static5	15.5	L	Static5	15.5	L

Table 2. Multiplexer assignments and pressure measurement locations for steady experiments.

Figure 4 is a schematic diagram of the optical system used to generate the schlieren images. Light from a Xenon flash lamp (Xenon Corp Nanopulser model 437B) focused on a pinhole that in turn acted as a point source of illumination for the experiment. This point source was placed at the focal point of a parabolic mirror so that the reflected light was collimated. The collimated beam was passed through the test section via two flat mirrors and collected by a second parabolic mirror which focuses the beam on a knife edge.The knife edge was oriented

horizontally in order to image density gradients normal to the free stream in the test section. A 400-mm lens re-collimated the beam downstream of the knife edge. Density gradients in the test section were imaged using a 105-mm lens and a standard 35-mm camera. A bellows was required to focus the image onto the back plane of the camera. Since the camera shutter was much slower than the phenomenon being investigated, it was held open manually for the duration of the experiment. Kodak Tmax400 film was used, exposed and developed normally.

Construction and Operation of Disturbance Generator

Figure 5 is a detail of the disturbance generator. An adjustable horizontal slot 0.040 in wide was located 15.5 in downstream of the splitter plate in the upper tunnel wall. The slot was oriented perpendicular to the flow and forms the bottom of a vertical shock tube installed as shown in Figure 1. The shock tube was 2.25 inches in diameter with driving and driven section lengths of 19.7 inches and 9.8 inches respectively. It was sized to provide a pulse of approximately 1.5 ms duration. The diaphragm was a mylar film of 0.005-mm thickness. When the tube fired, a well defined pulse was introduced perpendicularly to the main flow in the tunnel perturbing the thickened boundary layer and initiated possible formation and disgorgement of shock structures in the test section.

An x-t diagram of the shock tube firing is shown in Figure 6. The experiment began by pressurizing the driver section of the shock tube until the diaphragm breaks at pressure P4, approximately 350 mmHg greater than P1, set by the static pressure in the test section of the tunnel. Rupture of the diaphragm caused a shock to propagate through the driven gas toward the slot in the tunnel wall. About 0.02 ms after diaphragm rupture, the shock front passed a piezoelectric pressure transducer in the driven end of the shock tube near the slot. The signal from this transducer triggered the high-speed A/D converter and sampling of all PCB pressure transducers began. The experiment was performed in the reflected shock region (5).

The signal from the high-speed pressure transducer in the shock tube also triggered the Xenon lamp of the Schlieren system. The signal, sent to a high input impedance zero crossing circuit, triggered a variable delay generator (SRS DG535) which in turn triggered the Xenon lamp. By repeating the experiment with different time delays a series of Schlieren images representing the temporal evolution of the unsteady flow was accumulated.

Figure 7 shows a schematic drawing of the apparatus used to calibrate the pressure transducers. This process began by connecting an evacuated gas bottle to three pressure transducers and a high precision mercury manometer. The manometer pressure was recorded and the computer recorded signals from the pressure transducers. The valve C was then cracked, allowing the pressure in the manifold to rise, and another manometer reading and scan of the pressure transducers made. This process continued until the pressure in the manifold reached atmospheric. Figure 8 gives typical results of a calibration. The x-axis shows the voltage output of the pressure transducer normalized by the reference voltage used to drive the transducer; the y-axis shows the applied pressure in mmHg. Note that the responses are linear but each transducer has a different maximum operating pressure.

Data Collection

Because the time scales of the phenomena under investigation in the unsteady experiments were of the order of milliseconds, the experiment was automated. The most challenging aspect was manually synchronizing opening the camera shutter and firing the shock

tube so as to minimize the time the shutter was open. This arrangement was accepted because of the uncertainty of the diaphragm burst time and the relatively slow response of the camera shutter. As a consequence considerable care was exercized to block all light sources in the tunnel area.

Three types of data were collected in this experiment: pressure-time histories, static pressures, and Schlieren images. The Schlieren photographs were processed by a photo laboratory. The static pressure data was processed using various special-purpose computer programs written to account for the calibration of each pressure transducer and to perform iteration when required to compute shock Mach numbers. A certain amount of averaging occured when the data were collected as each transducer was polled 50 times for each data point and the average and standard deviation were recorded in each raw data file. Additional averaging occured after data collection when the results of different runs at the same conditions were averaged together.

The analysis of the pressure-time data from the high speed pressure transducers was the most complex because of the way the high speed A/D system worked. At the beginning of an experiment the system was turned on, and began scanning the acquisition channels and storing the data in an on-board buffer. At some time later the shock tube was fired, and the board was triggered. At this point the board read a user-specified number of points and dumped the data into a file. The advantage of this system was that since the on-board buffer had been continuously filling itself with data, when a trigger occured and the experiment stoped, pre-trigger data were left in the buffer and could be saved to the disk along with the post-trigger data. The drawback was that since the trigger time was uncertain, the channel, and consequently the pressure measurement corresponding to $t = 0$, changed from experiment to experiment. Thus the averaging procedure was required to account for the fact that the time-stamp of pressure data on channel 1, for example, changed from experiment to experiment.

Steady State Performance With Thick Boundary Layer

In order to analyze details of the transient behavior of the flow, it was necessary first to characterize the steady flow in the test section. Of particular interest were the boundary layer thicknesses on the upper and lower walls, the Mach number profile through the shear layer separating high and low speed flows, and the disturbance associated with the trailing edge of the splitter plate. It was especially important that this and other disturbances upstream of the shock tube be minimized so that effects of the disturbances that propagate upstream could be recognizable. Two methods were used. First, pitot traverses were made across the test section at two locations, one upstream and one downstream of the disturbance generator. Second, a series of static pressure measurements was made before each unsteady experiment at several points along the upper and lower walls of thse test section.

Figures 9 and 10 show static pressures in various parts of the test section as a function of the boundary layer injection valve position. Referring to the pressure tap locations shown in Figures 2 and 3, it is clear that the static pressure increased with downstream distance and that the static pressures were lowest with the injection valve set 1/2 turn open. Note also that this setting seems to correspond to the best matching of static pressures near the splitter plate exit with those of the incoming supersonic flow. As an additional check the expected pressure at the jet exit, based on the injection mass flow rate, was calculated and compared with the static pressure measurements in the tunnel, Figure 11. Although the data were noisy, it is clear that the best pressure match occured with the valve 1/2 turn open. The injection mass flow rate and the local static pressure also allowed computation of the injection Mach number, and these results are plotted in Figure 12.

Figures 13 and 14 are plots of the Mach number profile across the test section for an injection valve setting of 1/2 . In these plots y is zero at the upper wall and increases as one moves down from the upper to lower walls. The subscript on the Mach number M refers to the static pressure measurement used to compute the Mach number. Although the curves are similar in shape, the magnitudes differ. The values shown in Figure 12 probably are the better estimates of the Mach number distribution in the boundary layer.

When the shock tube was opened, allowing a continuous jet to issue from the disturbance slot, it was anticipated that a significant alteration of the steady flow in the tunnel would follow. Figures 15 and 16 show that pressures in the tunnel increased substantially and became insensitive to the boundary layer injection valve setting. The initial static pressure in the test section, static 5, rose far above the value corresponding to Mach 2.5. These data provided firm evidence that the tunnel was stalled under these conditions and suggested that the flow provided by the disturbance generator was sufficient to stall the tunnel for the unsteady experiments.

Because of the very thick boundary layer that was generated on the tunnel upper wall, the pressure probe exerted an unusually strong effect on the steady flow field. Consequently static pressures were also measured before each unsteady run to characterize the pressure distribution with the pressure probe removed. Plotting the various pressures as a function of injection valve setting, Figure 17, shows trends similar to those observed in the pitot traverse data. Again, an injection valve setting of 1/2 corresponded to the best matching of static pressure between the injected boundary layer and the main flow.

Experiments with Unsteady Flow

Based upon the experience with steady flow surveys, the unsteady flow experiments were conducted with the boundary layer injection valve setting of 1/2 open, leading to the minimum disturbance at the trailing edge of the separation plate, a boundary layer flow with a Mach number about 0.2, and a tunnel Mach number of 2.5. Figures 18 through 22 are a series of Schlieren images showing the propagation of a shock structure upstream into an initially supersonic flow. They were recorded with delays of 0.25 ms, 0.5 ms, 1.0 ms, 1.5 ms and 2.5 ms respectively, relative to the shock tube firing. In these images the flow moves from right to left toward the disturbance generator slot, visible on the far left edge of the upper wall. In the first image the jet of air from the shock tube is clearly visible as it issues into the enhanced boundary layer. Already a bow shock had formed upstream of the jet as the boundary layer flow turned down over the jet and into the free stream. In subsequent images this bow shock has propagated upstream through the subsonic boundary layer, thickening (and probably separating) the boundary layer in its wake, and appeared to strengthen as it moved.

Meanwhile another strong shock on the opposite wall became visible in the second image, t=0.5 ms and propagated upstream through the lower wall boundary layer in unison with the first, greatly thickening this boundary layer also. The "structure" of this shock strongly suggests nonuniformity across the working section, a condition to be expected in such a circumstance. The velocities of both shock structures were approximately 85 m/s, or Mach 0.35 with respect to the nominal Mach 2.5 condition in the test section.

The passage of these structures is clearly shown in the signals from the high speed pressure transducers mounted in the shock tube (0a) and the tunnel walls (1a, 2a, and 3a). Figures 23 through 25 show pressure time histories for each transducer. Beginning with the shock tube, Figure 23 shows that the diaphragm burst pressure was about 110 psi over the ambient tunnel pressure and that the pressure pulse lasted for approximately 2.5 ms. This was a long and strong pulse in comparison to the characteristic pressure fluctuations and time scales in

the test section. While Figure 24 shows a relatively weak disturbance propagating downstream of the jet, Figure 25 shows the passage of a very strong disturbance upstream through the boundary layer about 1 ms after shock tube firing. This strong disturbance corresponded to the first shock wave seen in the Schlieren images.

Finally, Figure 26 shows a series of strong disturbances that swept across the pressure transducer on the opposite side of the wall downstream of the jet. The record of this strong disturbance was unlike measurements from the other transducers, which showed the passage of a single disturbance with a relatively stable region of high pressure in its wake. Comparing the time history of these disturbances to the pressure in the shock tube, it is clear that the disturbances were directly related to the reflections in the shock tube. Initially, as the pressure rises, a jet emerged into the main flow, caused the boundary layer to separate and forced a severe distortion of the main flow. The second pressure pulse in the shock tube generated a second jet, which again disturbed the mean flow in the tunnel. Presumably the cycle continued until the pressure oscillations in the shock tube were damped out. It should be recalled that these plots represent an average of the data for 45 individual shots, indicating that the phenomena are very repeatable.

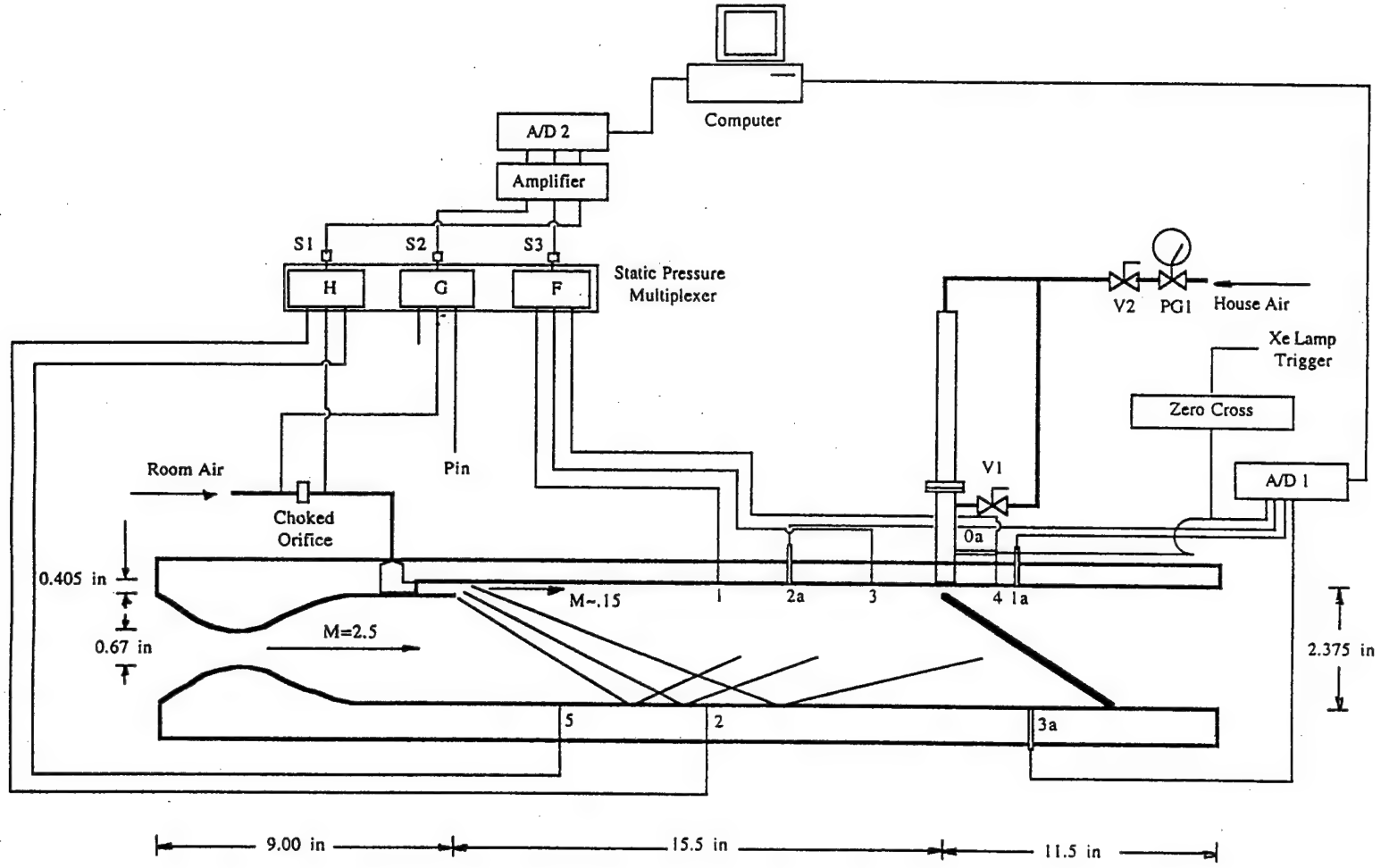

Figure 1. Tunnel Configuration for Unsteady Pressure Measurements

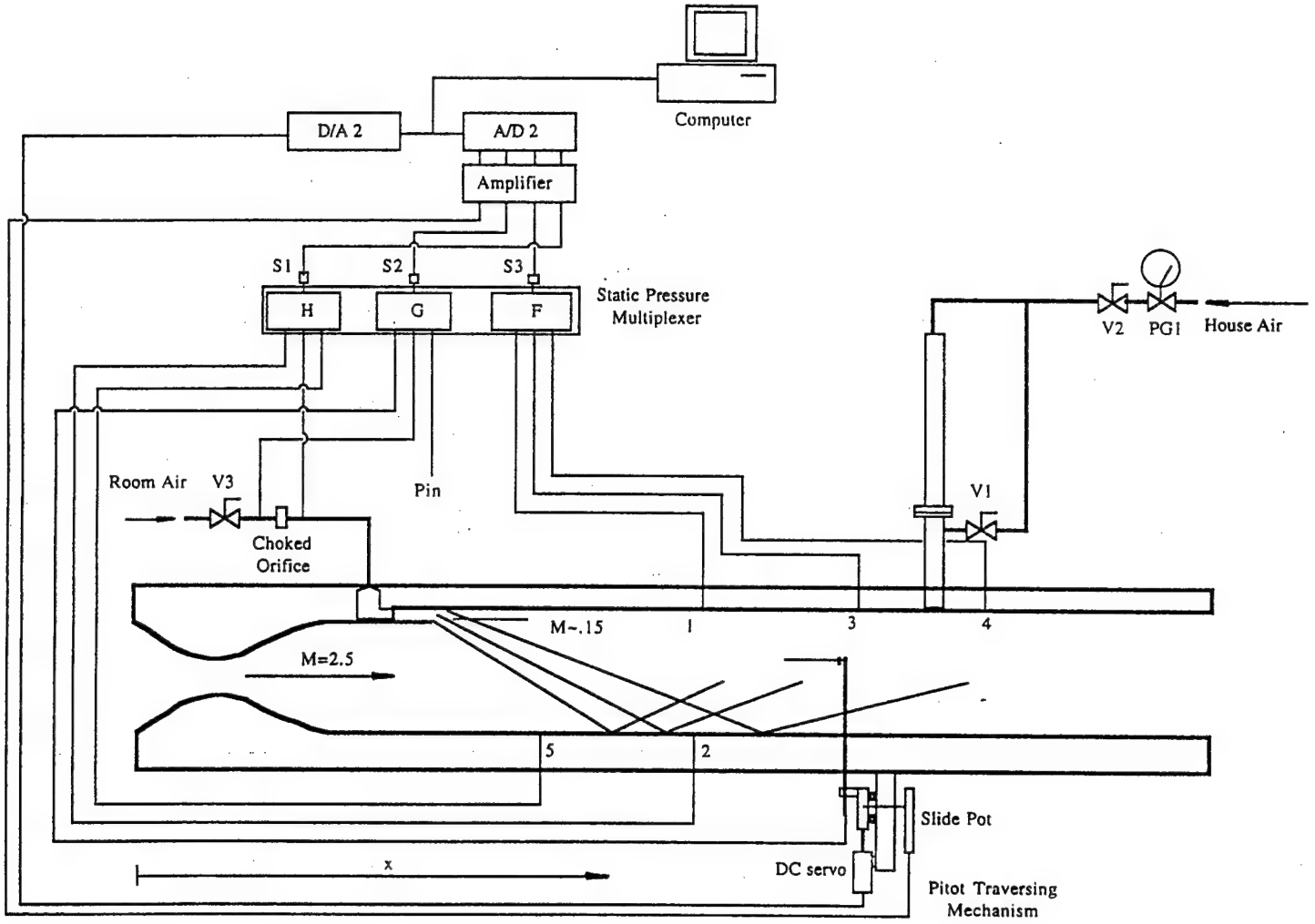

Figure 2. Tunnel Configuration for Second Series of Pitot Traverses

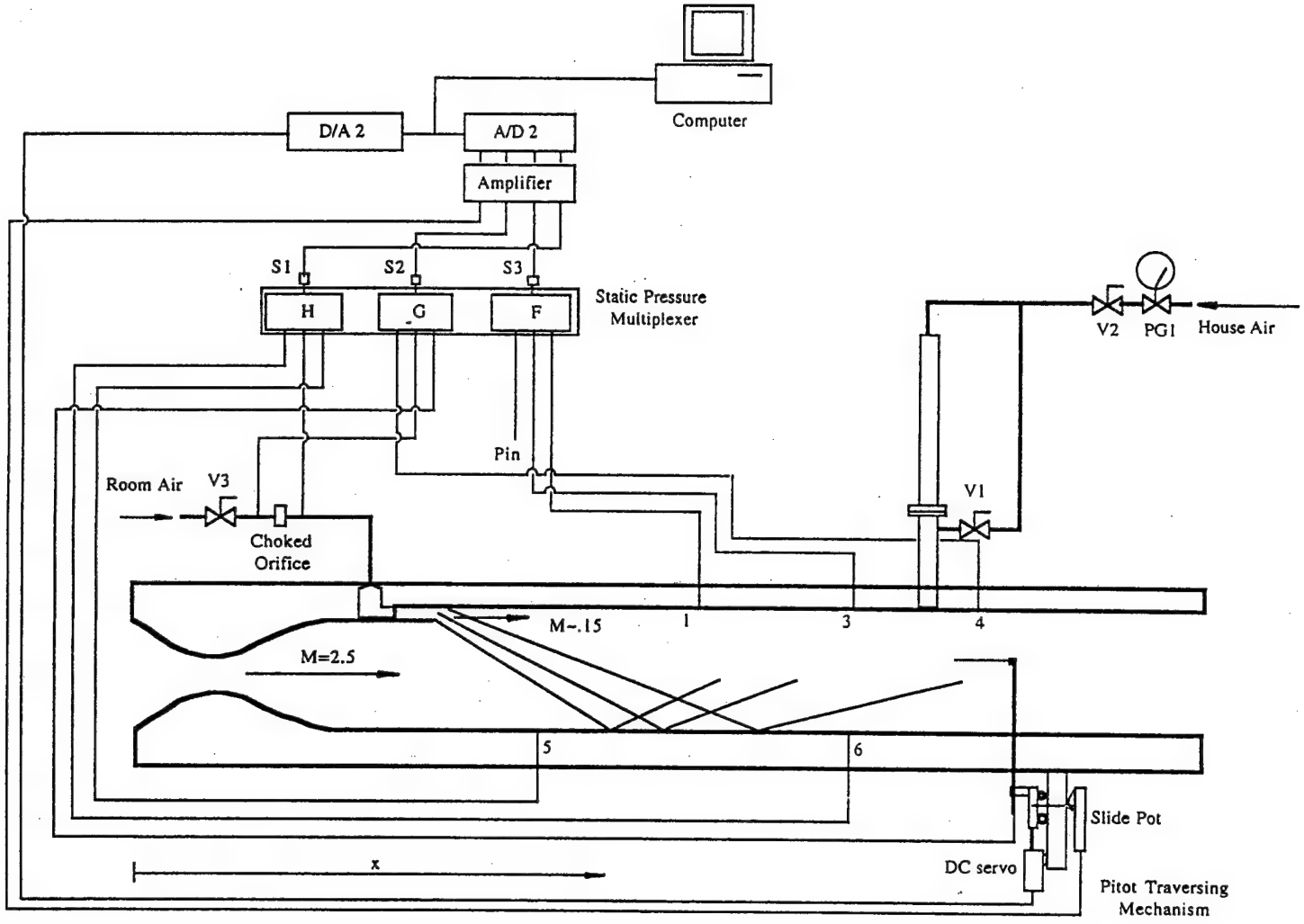

Figure 3. Tunnel Configuration for First Series of Pitot Traverses

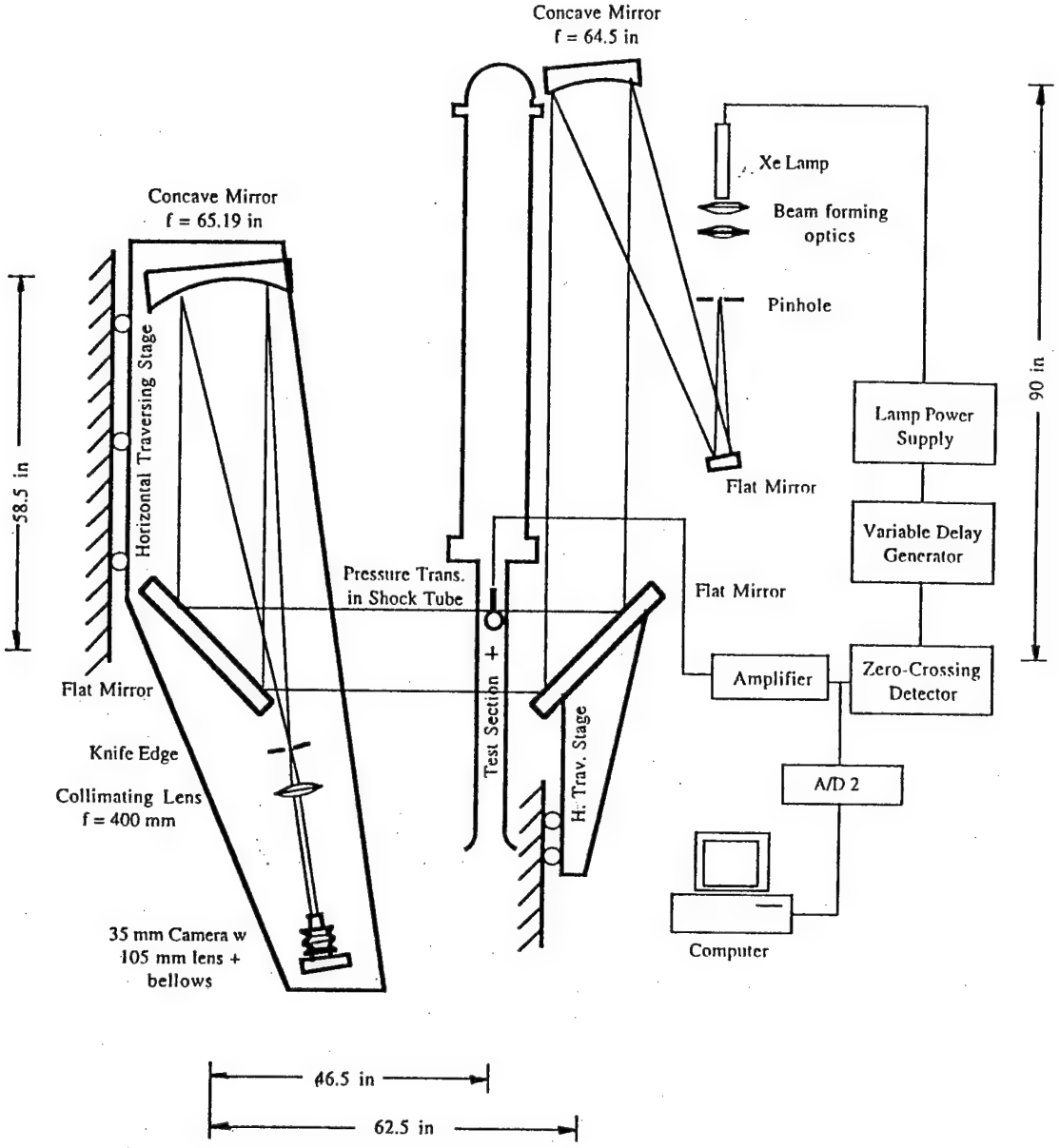

Figure 4. Optical Arrangement for Schlieren Photography

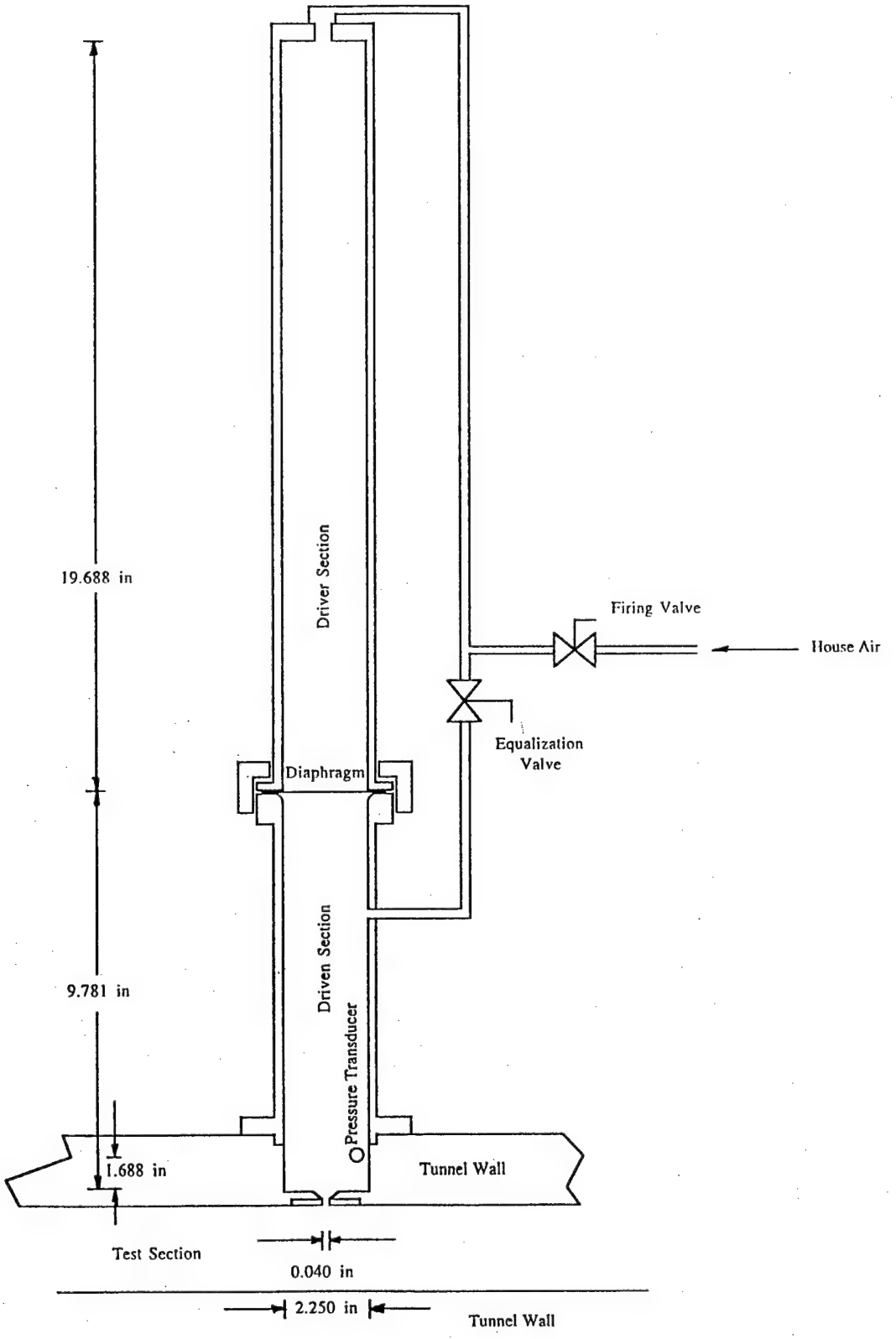

Figure 5. Diagram of Disturbance Generator

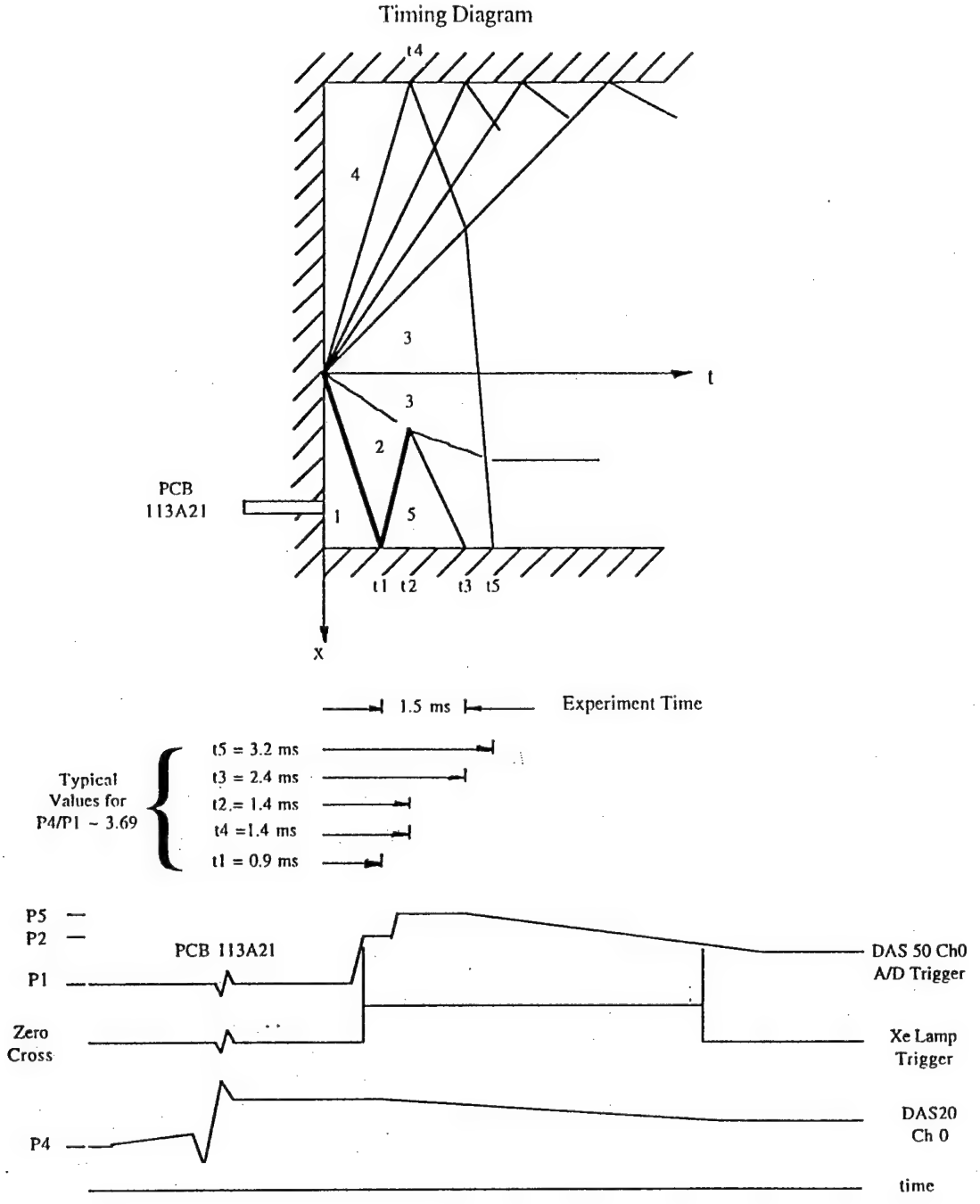

Figure 6. Timing Diagram for Signal Generator

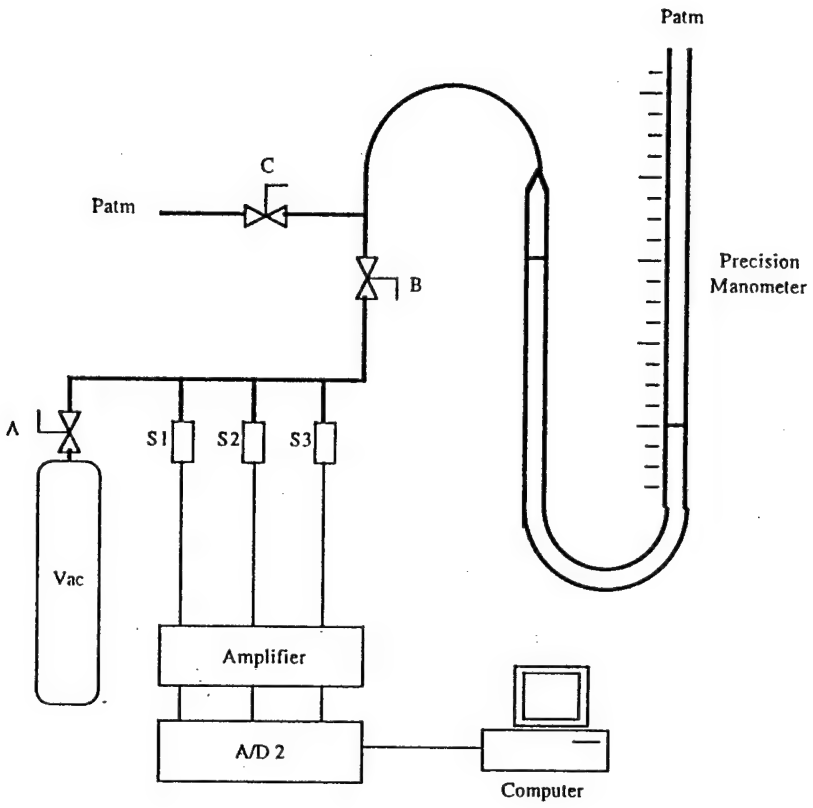

Figure 7. Arrangement for Pressure Transducer Calibration

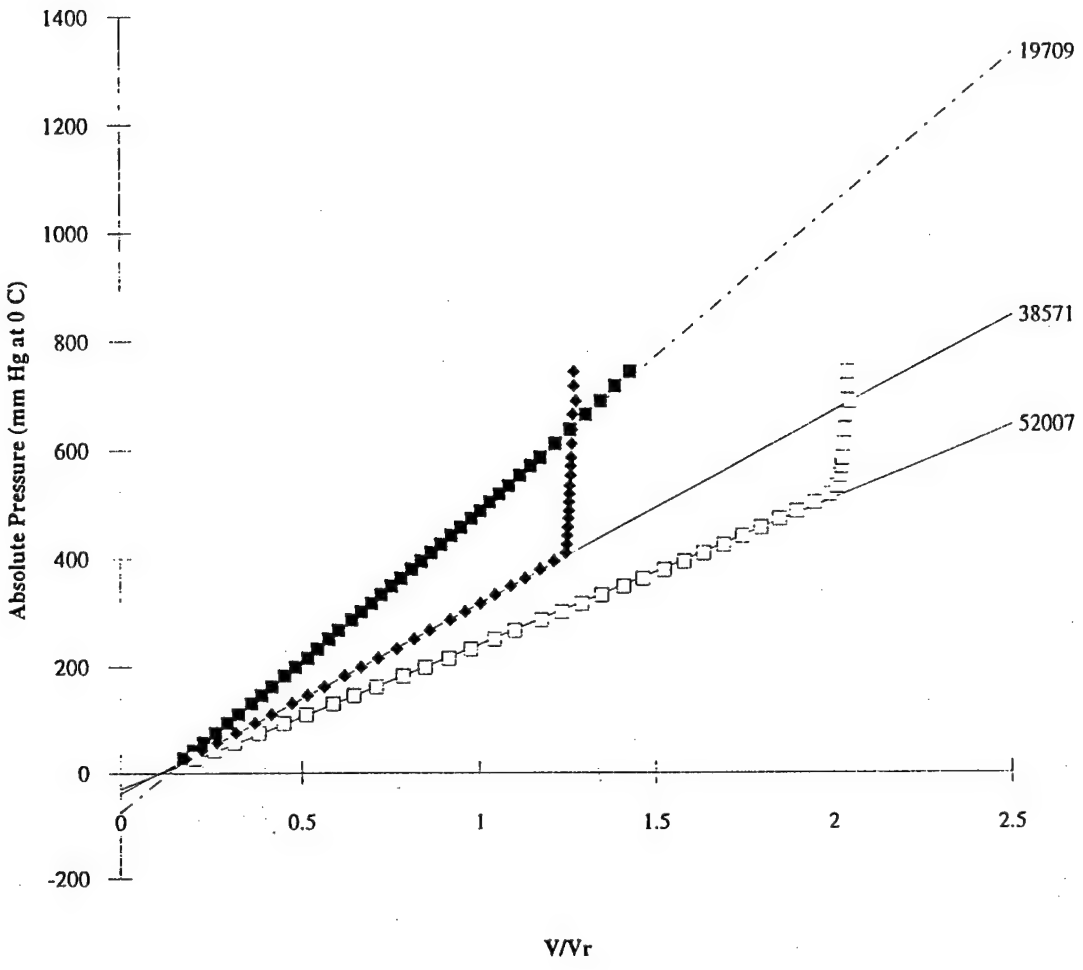

Figure 8. Statham Pressure Transducer Calibration

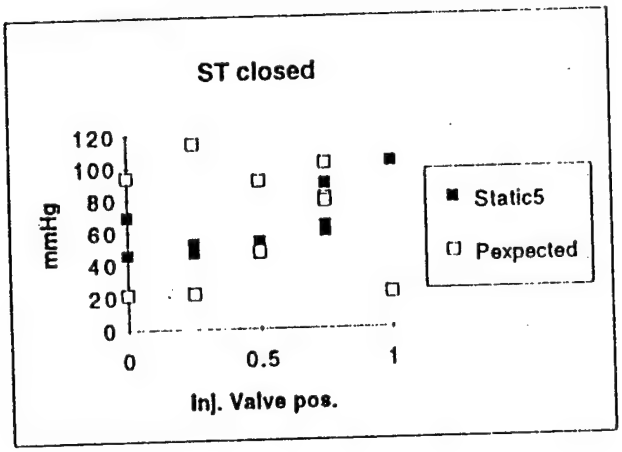

Figure 11. Comparison of Measured and Expected Static Pressure Measurements

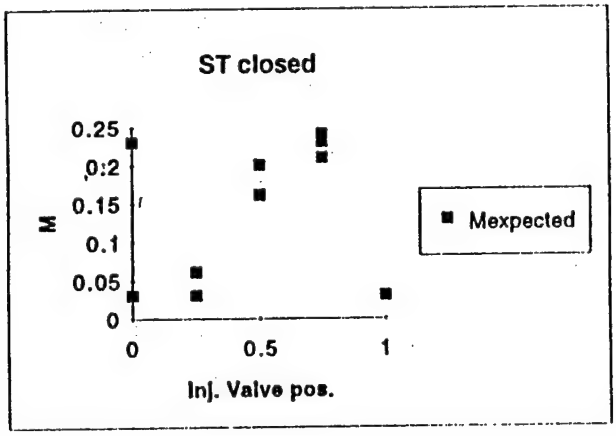

Figure 12. Boundary Layer Injection Mach Number from Flow Measurement

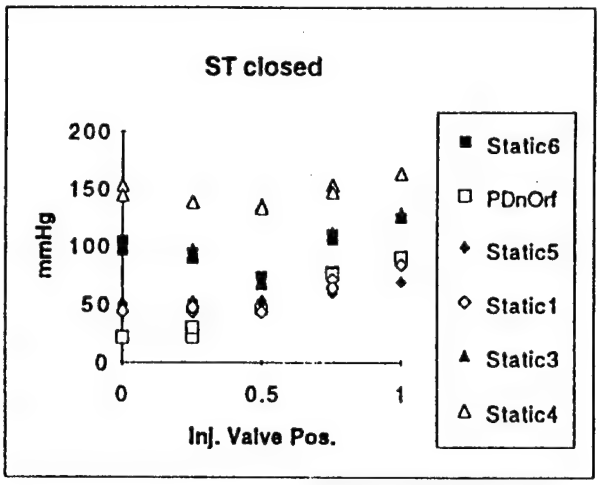

Figure 9. Wall Static Pressures for Various Boundary Layer Flow Rates

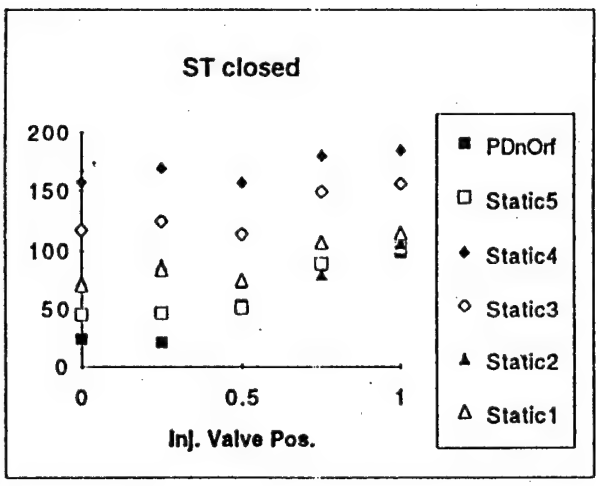

Figure 10. Wall Static Pressures for Various Boundary Layer Flow Rates

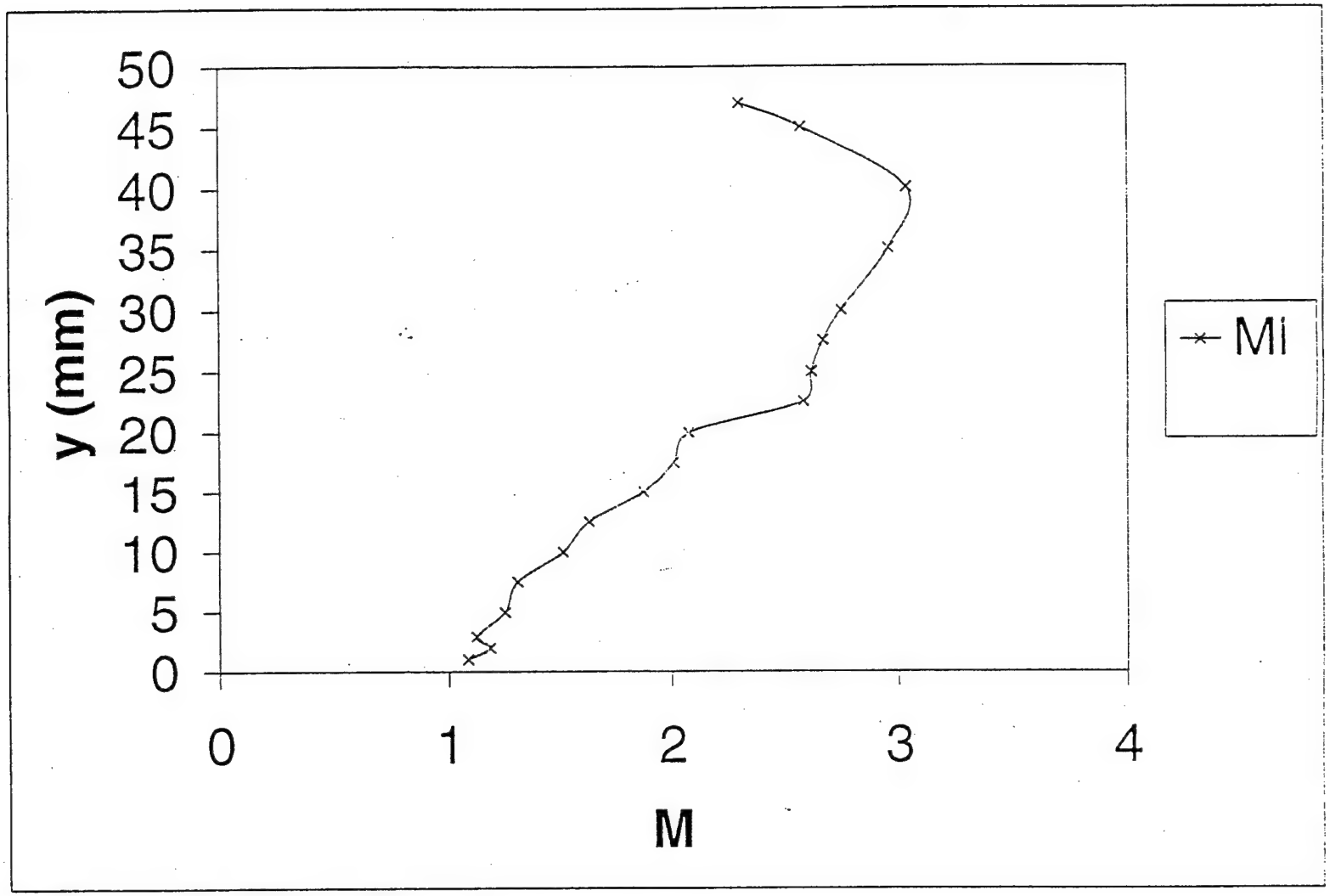

Figure 13. Tunnel Mach Number Distribution Using Lower Wall Static

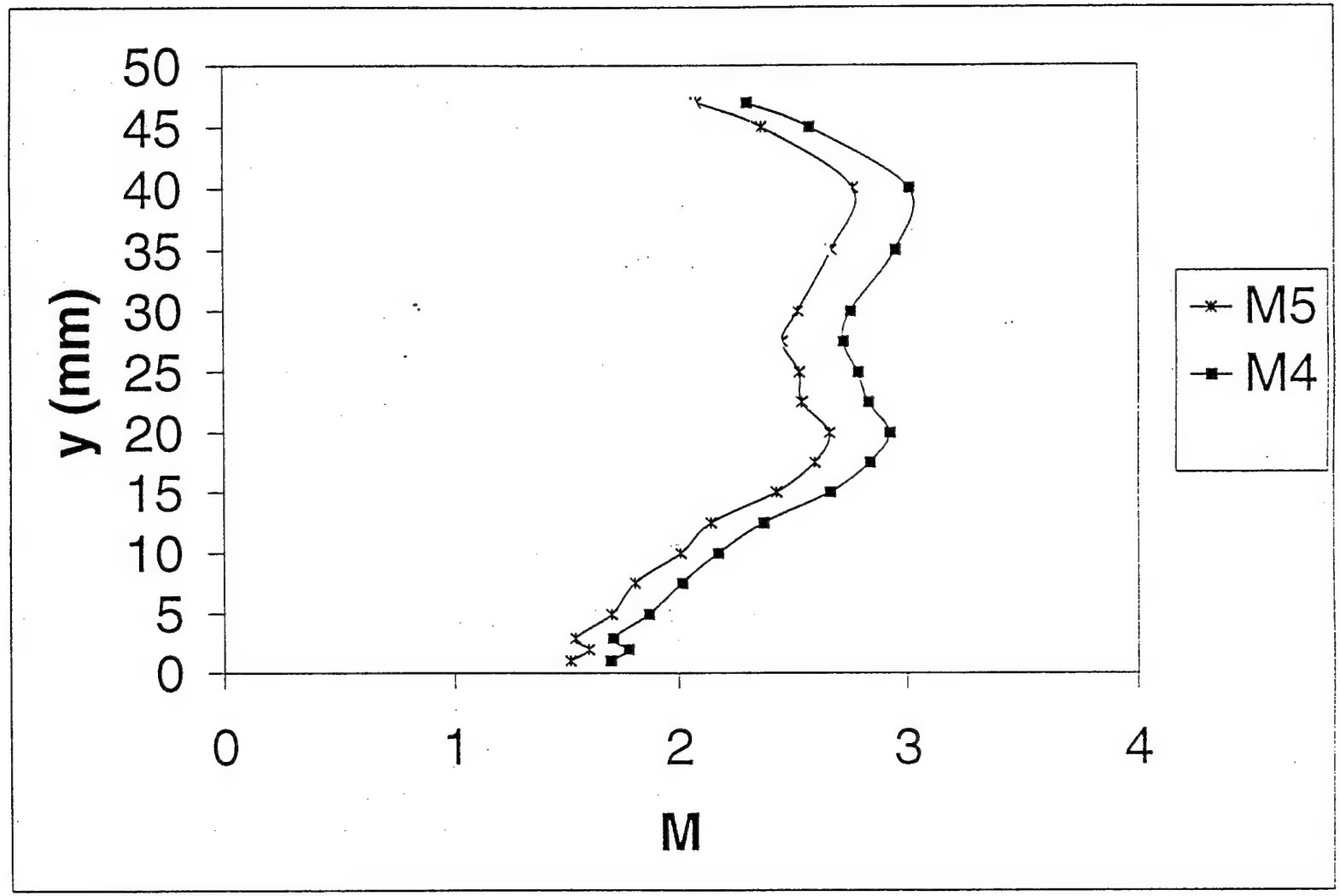

Figure 14. Tunnel Mach Number Distribution Using Static Taps Indicated

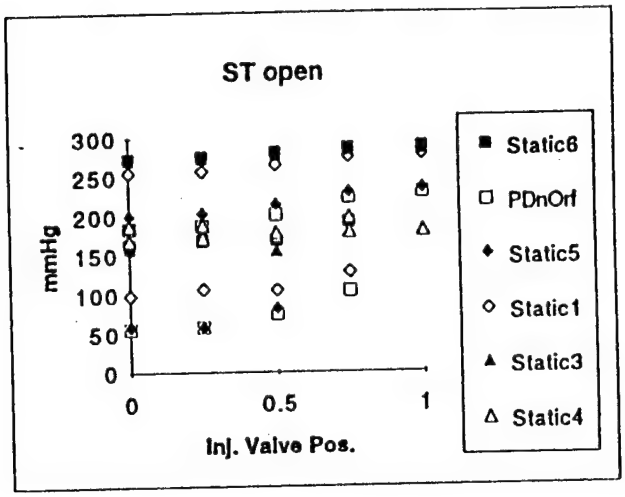

Figure 15. Pressure Distribution with Disturbance Slot Open, Tunnel Stalled

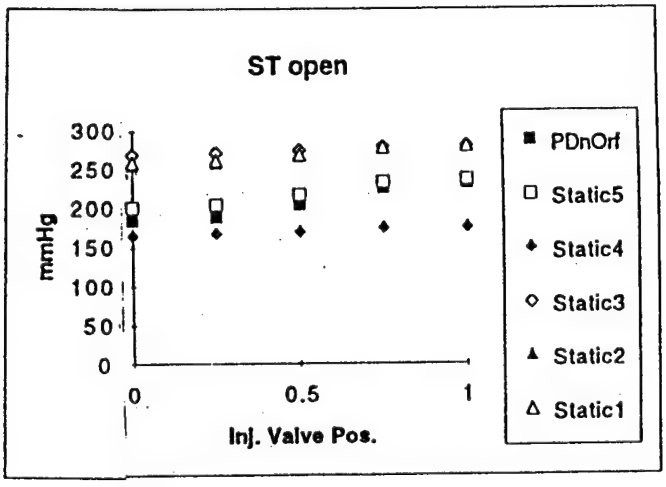

Figure 16. Pressure Distribution with Disturbance Slot Open, Tunnel Stalled

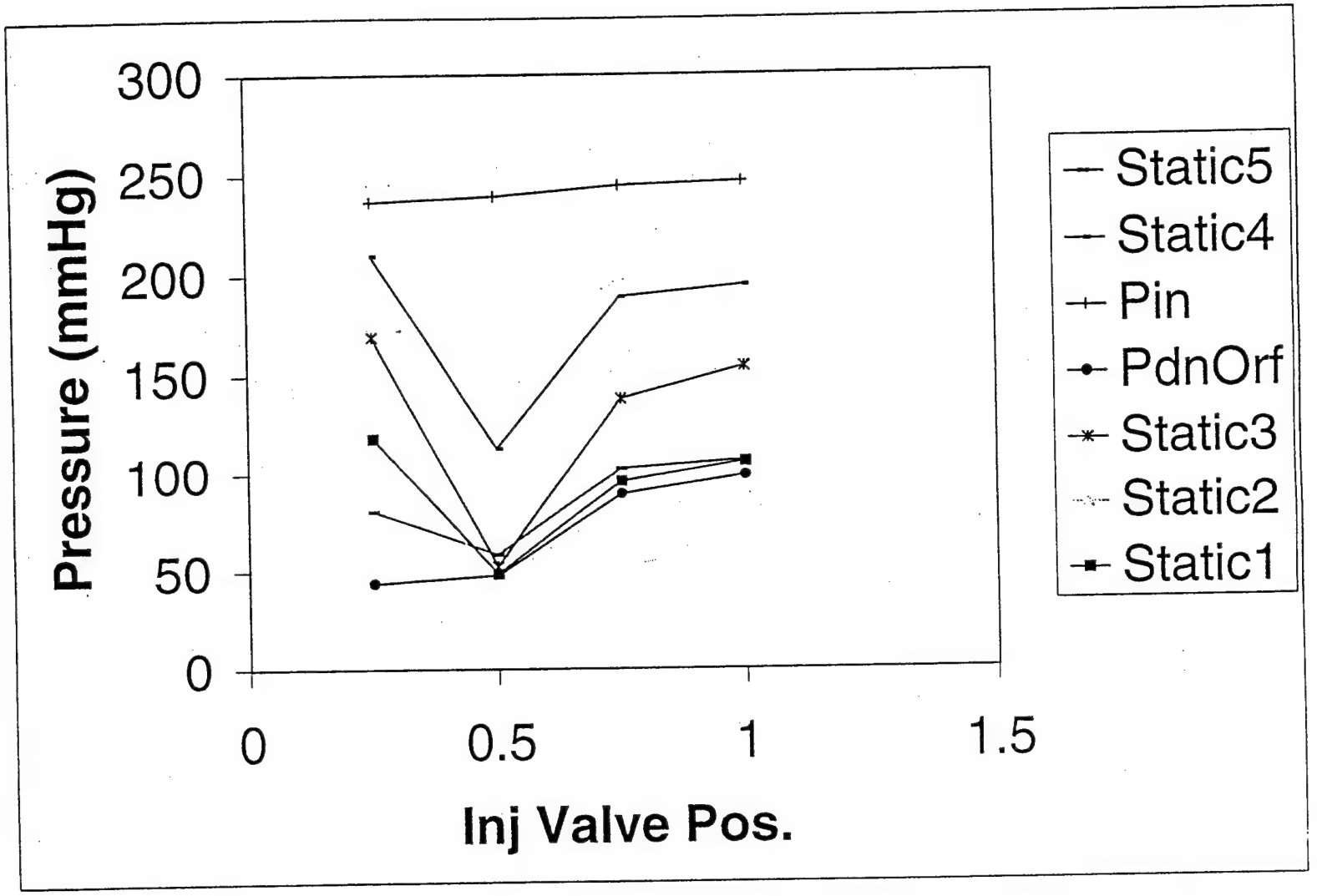

Figure 17. Static Pressures for Range of Valve Settings, Probe Removed

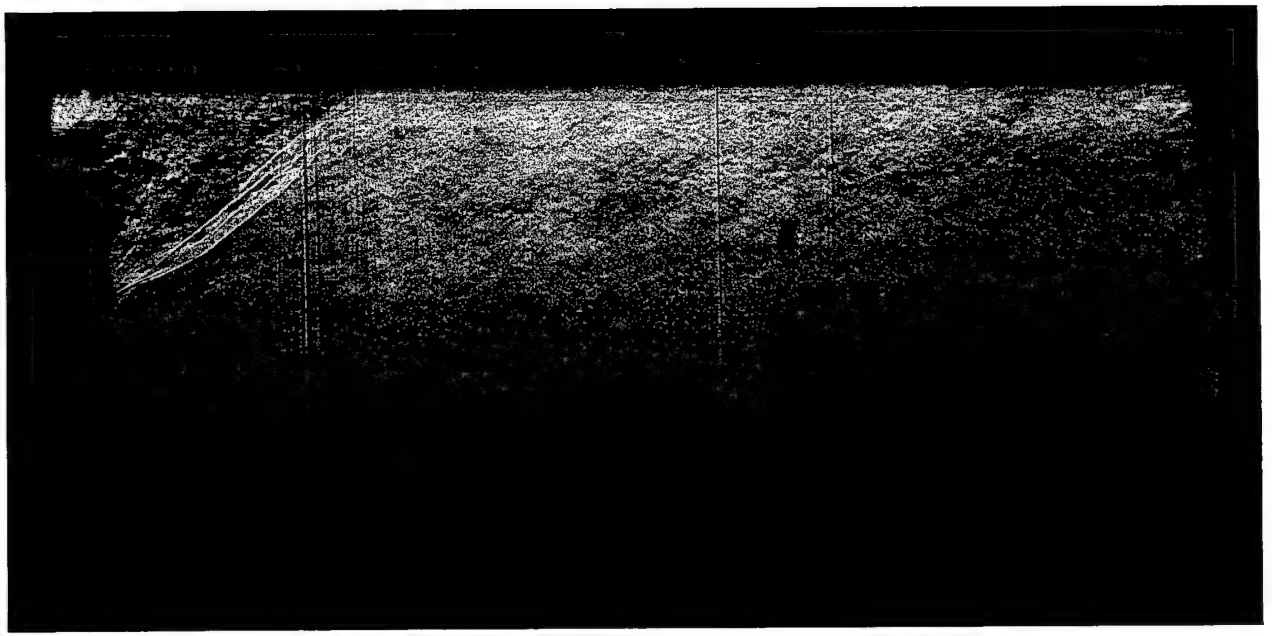

Figure 18. Schlieren Image of Propagating Shock Structure, 0.25 ms After Firing

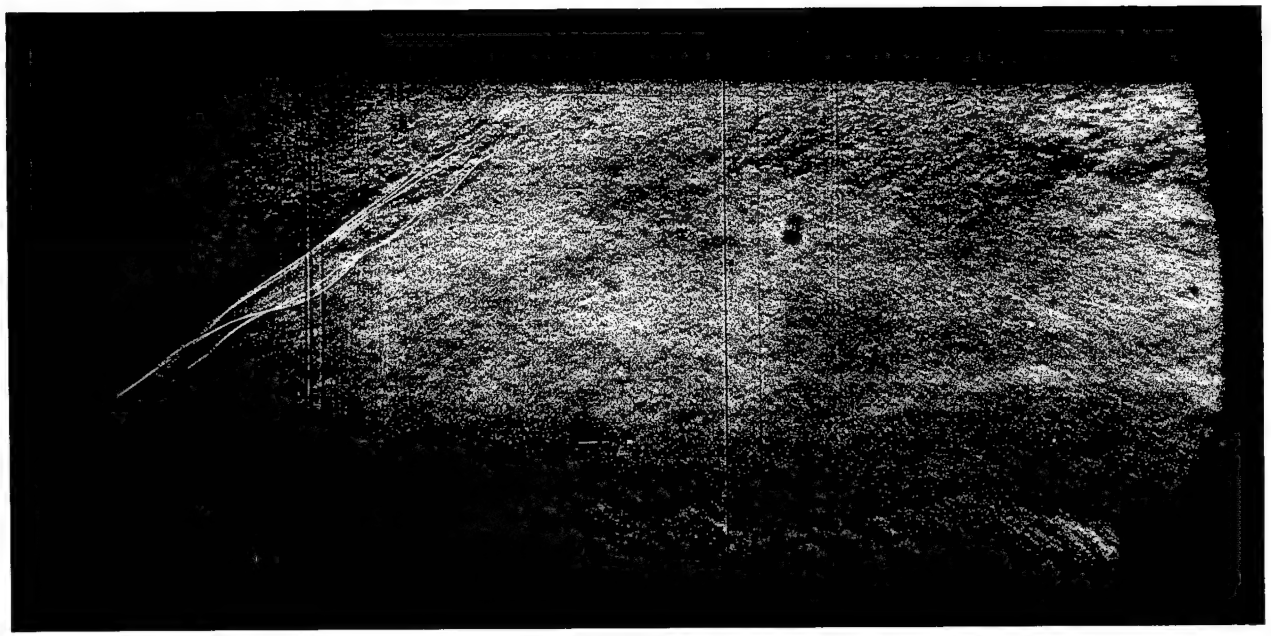

Figure 19. Schlieren Image of Propagating Shock Structure, 0.5 ms After Firing

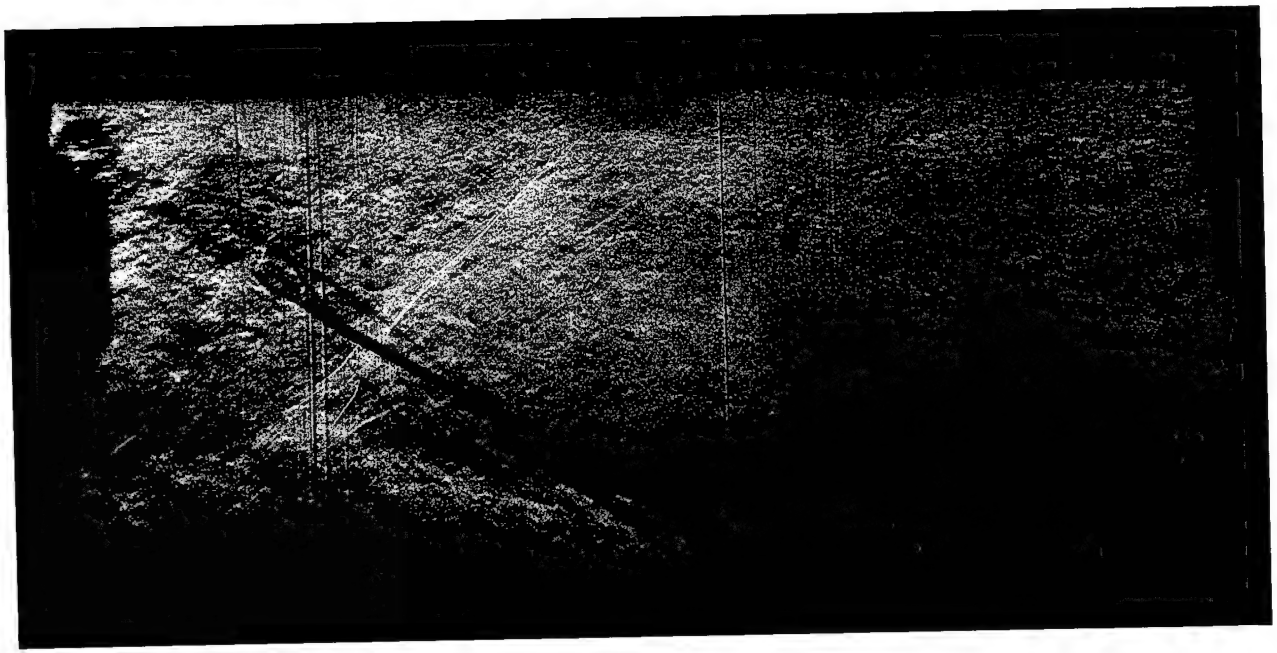

Figure 20. Schlieren Image of Propagating Shock Structure, 1.0 ms After Firing

Figure 21. Schlieren Image of Propagating Shock Structure, 1.5 ms After Firing

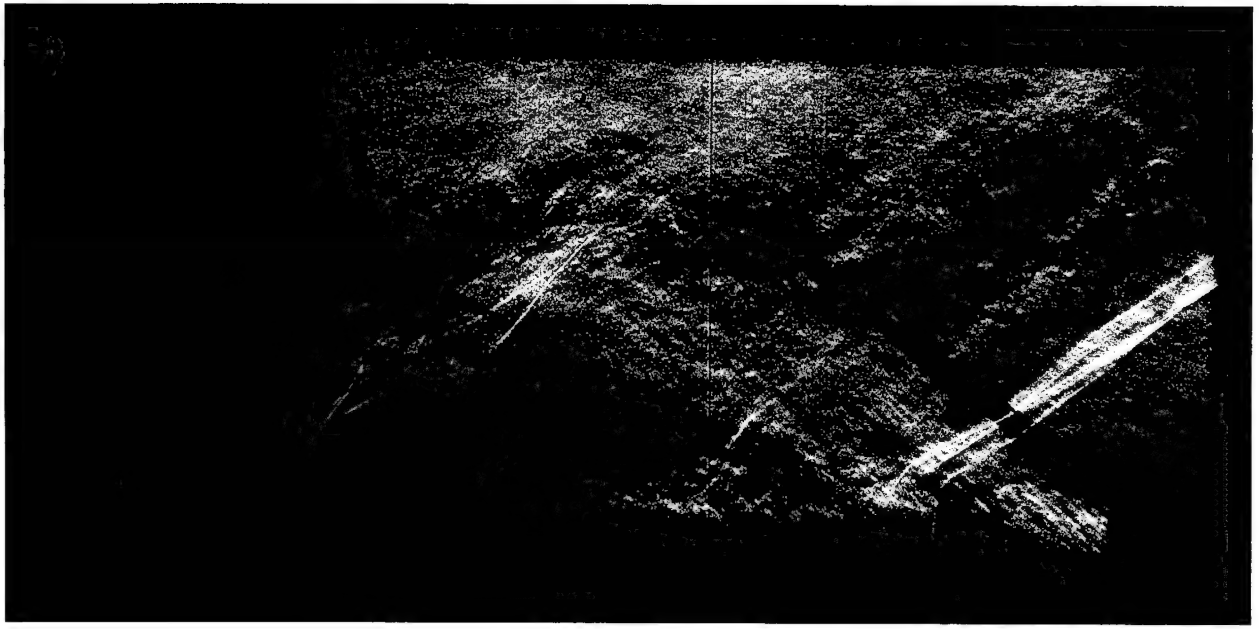

Figure 22. Schlieren Image of Propagating Shock Structure, 2.5 ms After Firing

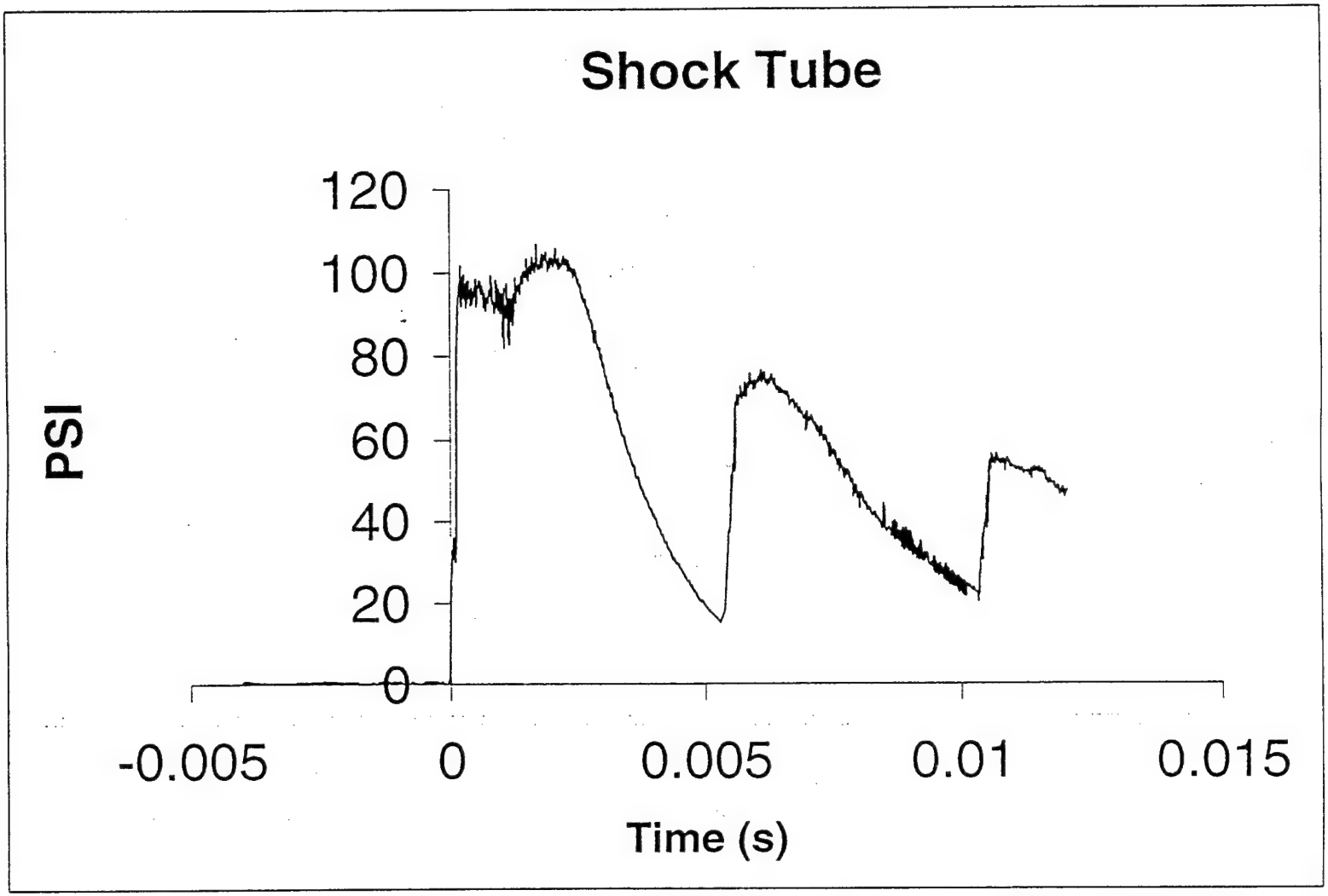

Figure 23. Response of High Speed Transducer 0a Located in Shock Tube

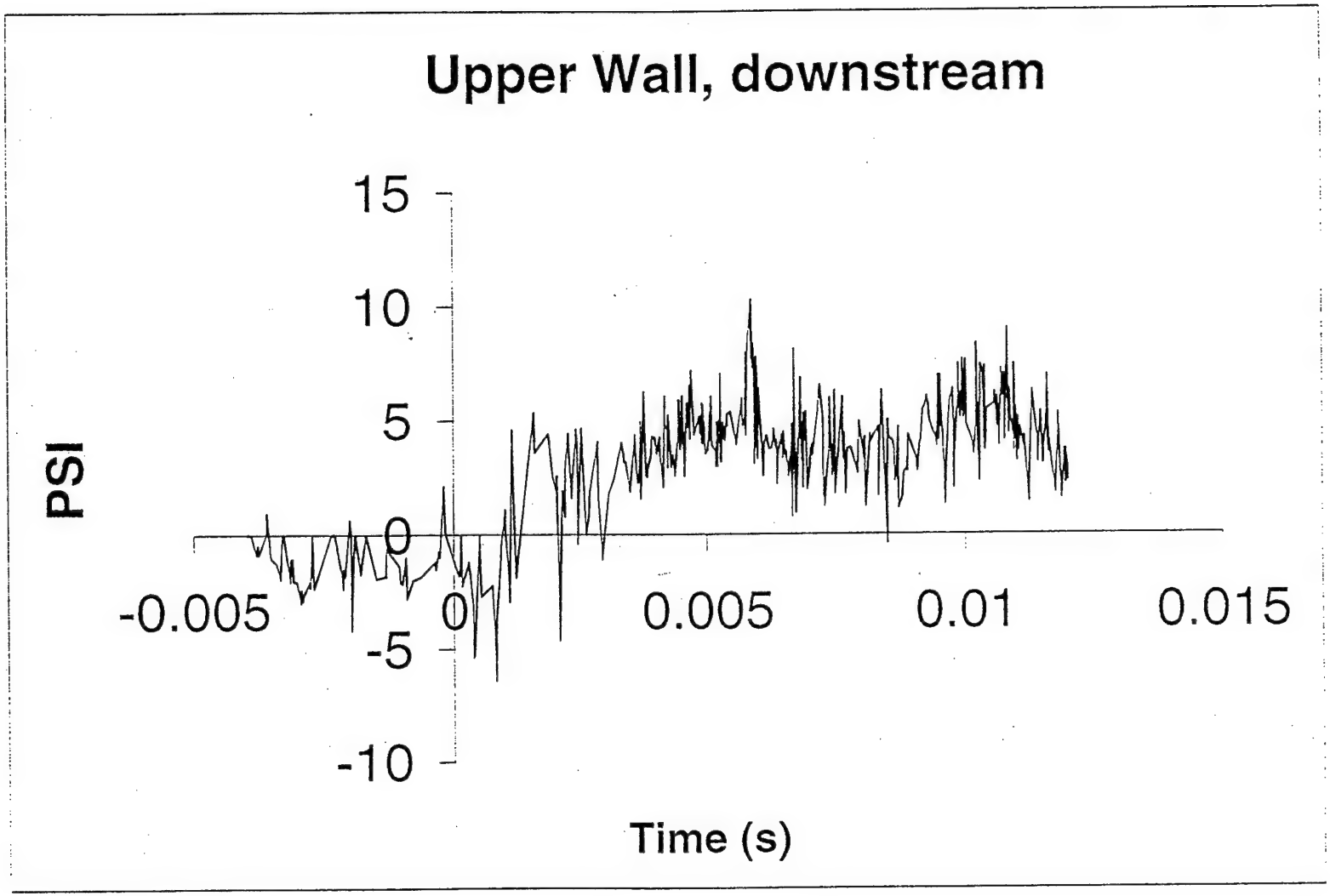

Figure 24. Response of Transducer 1a Located Downstream of Disturbance Slot

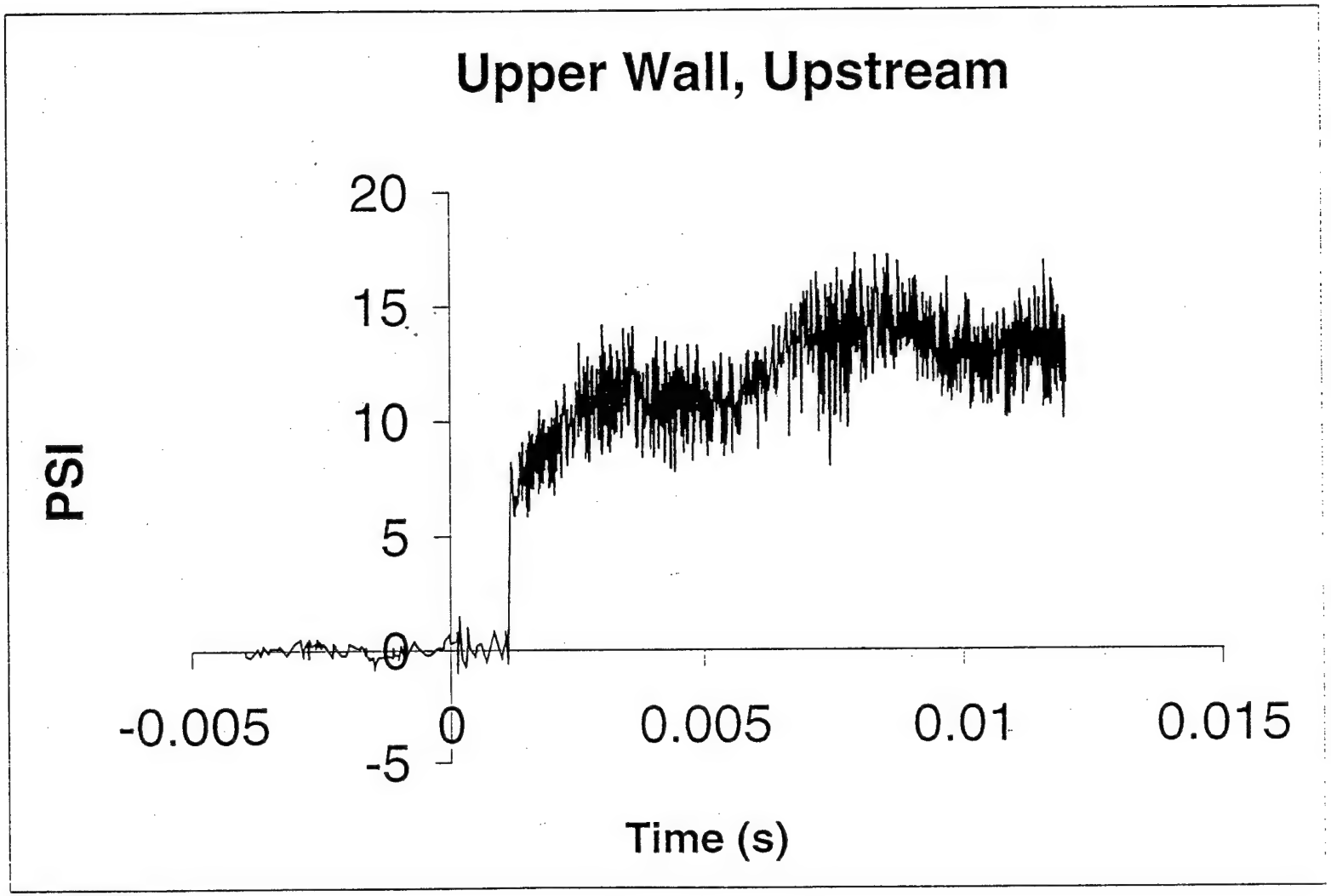

Figure 25. Response of Transducer 2a Located Upstream of Disturbance Slot

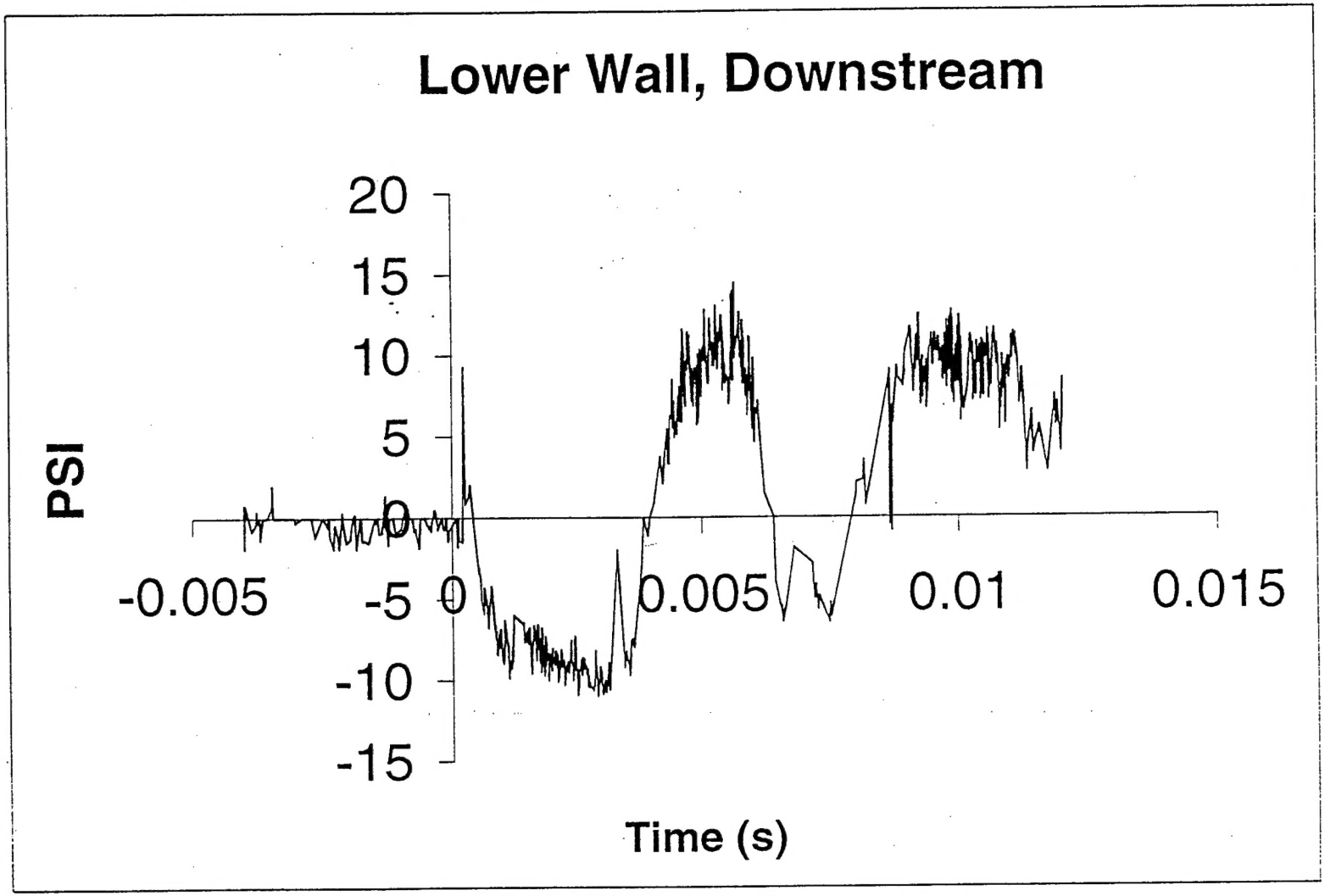

Figure 26. Response of Transducer 3a Located Upstream on Lower Wall

5. NOTATION

a,b	Coefficients in Matching Relations
A	Flow Cross section
D	Complex Area Disturbance Wave
i, j	Indices Indicating Element or Stream Number
k	Wave Number
K	Dimensionless Complex Wave Number, Eq. 9
m	Mass Flow Rate
M	Mach Number
p	Local Pressure
P	Real Part, Pressure Wave
Q	Imaginary Part, Pressure Wave
R	Real Part, Wave Number
S	Imaginary Part, Wave Number
t	Time
T	Gas Temperature
u	Gas Velocity
U	Complex Velocity Wave
V	Velocity of Pressure Waves
x	Horizontal Coordinate
′ (prime)	Perturbation Quantity
α	Eq. 16, Eq. 22
β	Eq. 18, Eq. 24
γ	Specific Heat Ratio
ρ	Gas Density
ϖ	Angular Frequency of Pressure Wave

6. PERSONNEL

Principal Investigator: Frank E. Marble, Professor (Emeritus) Mechanical Engineering and Jet Propulsion.

Edward E. Zukoski, Professor (Emeritus) Mechanical Engineering and Jet Propulsion. (Deceased, May 26, 1997)

Christopher Cadou, Post Doctoral Fellow, Jet Propulsion

7. PUBLICATIONS

None

8. INTERACTIONS

Frank E. Marble:

Member, Aeronautics and Space Engineering Board, National Research Council.

Member, Aeronautics Advisory Committee, NASA Headquarters.

Consultant, Gas Turbine Laboratory, Massachusetts Institute of Technology.

Consultant, Turbomachinery and Combustion, NASA-Lewis Research Center.

Member, Technical Advisory Committee, United Technologies Corporation, Pratt & Whitney Division.

Consultant, United Technology Research Center, United Technologies Corporation.

9. INVENTIONS

None

10. HONORS AND AWARDS

(Lifetime Achievement)

Frank E. Marble:

Fellow, American Institute of Aeronautics and Astronautics

Member, National Academy of Engineering, 1974

Member, National Academy of Sciences 1989

Edward E. Zukoski:

Fellow, American Institute of Aeronautics and Astronautics